Inorganic Chemistry

pubs.acs.org/IC

Article

Probing CO Generation through Metal-Assisted Alcohol Dehydrogenation in Metal-2-(arylazo)phenol Complexes Using Isotopic Labeling (Metal = Ru, Ir): Synthesis, Characterization, and Cytotoxicity Studies

Satabdi Roy, Monalisa Mohanty, Reece G. Miller, Sushree Aradhana Patra, Sudhir Lima, Atanu Banerjee, Nils Metzler-Nolte,* Ekkehard Sinn, Werner Kaminsky, and Rupam Dinda*

Cite This: https://dx.doi.org/10.1021/acs.inorgchem.0c02563

Read Online

ACCESS | Metrics & More | Article Recommendations | Supporting Information

ABSTRACT: The reaction of 2-{2-(benzo[1,3]dioxol-5-yl)- diazo}-4-methylphenol (HL) with $[Ru(PPh_3)_3Cl_2]$ in ethanol resulted in the carbonylated ruthenium complex $[RuL(PPh_3)_2(CO)]$ (**1**), wherein metal-assisted decarbonylation via in situ ethanol dehydrogenation is observed. When the reaction was performed in acetonitrile, however, the complex $[RuL(PPh_3)_2(CH_3CN)]$ (**2**) was obtained as the main product, probably by trapping of a common intermediate through coordination of CH_3CN to the Ru(II) center. The analogous reaction of HL with $[Ir(PPh_3)_3Cl]$ in ethanol did not result in ethanol decarbonylation and instead gave the organoiridium hydride complex $[IrL(PPh_3)_2(H)]$ (**3**). Unambiguous evidence for the generation of CO via ruthenium-assisted ethanol oxidation is provided by the synthesis of the ^{13}C-labeled complex, $[Ru(PPh_3)_2L(^{13}CO)]$ (**1A**) using isotopically labeled ethanol, $CH_3{}^{13}CH_2OH$. To summarize all the evidence, a ruthenium-assisted mechanistic pathway for the decarbonylation and generation of alkane via alcohol dehydrogenation is proposed. In addition, the in vitro antiproliferative activity of complexes **1**−**3** was tested against human cervical (HeLa) and human colorectal adenocarcinoma (HT-29) cell lines. Complexes **1**−**3** showed impressive cytotoxicity against both HeLa (half-maximal inhibitory concentration (IC_{50}) value of 3.84−4.22 μM) and HT-29 cancer cells (IC_{50} values between 3.3 and 4.5 μM). Moreover, the complexes were comparatively less toxic to noncancerous NIH-3T3 cells.

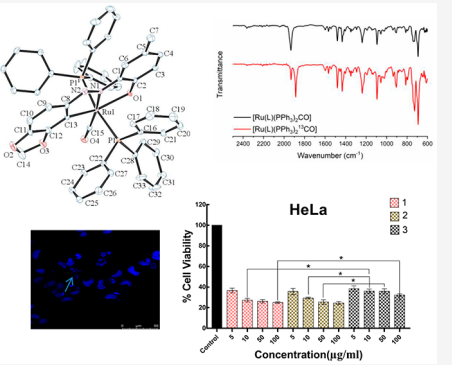

INTRODUCTION

The elimination of functional groups from organic molecules has immense significance in chemistry, including the synthesis of natural products.[1,2] In this context, decarbonylation reactions have become an indispensable aspect in the advancement of chemical synthesis. The key challenge of the decarbonylation reaction lies in the high bond dissociation energy of the C−C bond. Complexes of platinum group metals have been used to address this issue, as the metal center destabilizes the C−C bond through single- or two-electron-transfer processes. Hence, the platinum-group metals have drawn considerable attention over the decades.[3−5] Among the platinum-group metals, ruthenium exhibits the largest range of stable oxidation states (from −II to + VIII).[6] Hence, there is interest in the exploration of new ruthenium-based catalysts capable of decarbonylation reactions, especially after an initial report by Dolphin and co-workers on the stoichiometric decarbonylation using a ruthenium−porphyrin-based complex.[7] An iridium-catalyzed decarbonylation method has also been reported by Tsuji and co-workers, wherein a variety of functional groups were tolerated under mild reaction conditions.[8] In this way, effective synthetic decarbonylation processes can be beneficial for the generation of fuel-grade alkanes and should be attractive alternatives to existing expensive hydrogenation methodologies.[9] Bhattacharya and co-workers,[10] Jayanthi et al.,[11] and Dinger et al.[12] have worked on ruthenium complexes wherein in situ solvent oxidation and decarbonylation had led to CO-coordinated Ru(II) complexes. These groups had proposed CO generation via either Ru-assisted methyl oxidation or solvent oxidation in azo and hydrazone complexes. However, their findings lacked substantial experimental evidence to support the mechanism of Ru-assisted solvent oxidation. Thus, further experimental investigations into the precise mechanism of these Ru-assisted alcohol dehydrogenation reactions and CO coordination are needed.[11,12] These literature reports prompted us to synthesize some new ruthenium azo complexes and examine the possible

Received: August 27, 2020

solvent oxidation (by using ^{13}C-labeled ethanol) and subsequent decarbonylation. We here focus on the synthesis of organometallic ruthenium complexes (**1** & **2**) derived from arylazo functionalized ligands, wherein an in situ solvent oxidation and subsequent decarbonylation to generate an alkane would be possible. To further see whether this decarbonylation is specific for ruthenium, we attempted to observe similar in situ decarbonylation in an organoiridium complex (**3**) using the same organic ligand.

However, it is also known that arylazo complexes of the platinum-group metals have been the subject of substantial interest because of their rich redox and spectroscopic behavior, catalytic activities, and isomerization reactions.[13−16] By comparison, the anticancer activity of platinum arylazo complexes has received rather limited attention.[17a−c] While conventional platinum anticancer drugs such as cisplatin, carboplatin, and oxaliplatin are potent against a range of tumors, their side effects like toxicity toward normal tissue and tumor resistance have motivated researchers to develop anticancer agents that diverge from the stereotypical complexes already in use.[17d−f] In this direction, ruthenium and iridium complexes have emerged as encouraging classes of metallodrug candidates and hold great promise for cancer chemotherapy.[18] Moreover, recent reports have revealed ruthenium complexes as remarkable antiproliferative agents, for example, the Ru(III)-based anticancer drugs indazolium *trans*-[tetrachlorobis(1*H*-indazole)ruthenate(III)] (KP1019),[19] its sodium salt analogue sodium *trans*-[tetrachlorobis(1*H*-indazole)ruthenate(III)] (NKP-1339),[20] and the new antimetastasis inhibitor imidazolium *trans*-[tetrachlorobis(1*H*-imidazole)(*S*-dimethyl sulfoxide)-ruthenate(III)] (NAMI-A),[21] which all have proceeded into the clinical stages of drug development. Furthermore, iridium complexes have been reported to generate reactive oxygen species and to induce apoptosis by acting on mitochondria as well as exerting anticancer effects through interaction with DNA.[22−24]

Phenylazo ligands have a crucial role in cytotoxicity against the A2780 ovarian and A549 lung-cancer cell lines as reported by Dougan et al. during investigation of η^6-areneruthenium(II) derivatives containing phenylazo ligands.[17a] The azo derivatives of ruthenium were found to be more cytotoxic as compared to the oxadiazole derivatives, on human glioblastoma cell lines, inspiring further study of azo-coordinated complexes.[17c] The redox reactions of the metal-coordinated azo ligands have been known to increase the cytotoxicity of half-sandwich organometallic (arene)-ruthenium(II) complexes.[17a,c] As compared to the free arylazo ligand, the transition-metal chelated azo complexes target cancer cells better than normal cells due to increased lipophilicity on chelation; this prompts the design and exploration of more metal-coordinated azo compounds.[25] Significant in vitro cytotoxic results of azo-vanadium complexes have also been reported in our earlier works, which further stimulates us to design and study azo-functionalized complexes.[26] Another class of pharmacophoric interest are triphenylphosphine (PPh_3)-coordinated metal complexes, as they exhibit excellent potential in chemotherapy by influencing mitochondrial metabolism.[27a−g] Using hydrophobic PPh_3-ligated complexes results in complexes with good cytotoxicity, presumably due to their increasing vehiculation property.[27h−j] Some ruthenium phosphine complexes are known to inhibit the human topoisomerase IB enzyme (a potential biological target for complexes).[27h] It has been demonstrated that the presence of a PPh_3 ligand is important also to facilitate the binding of the Ru complex to DNA and then distort its secondary and tertiary structure.[27j,k] Also, wide investigations of platinum, ruthenium, copper, and gold complexes have led to conclusions that mixed-ligand complexes possessing PPh_3 are highly cytotoxic in contrast to the phosphine-free ones, which inhibited cell proliferation only in relatively high concentrations.[27h,l−q] Thus, the wide cytotoxic activity of azo- and PPh_3-derived complexes stimulated us to investigate mixed azo- and PPh_3-coordinated complexes.

Herein, we report the synthesis of organoruthenium(II) (**1** and **2**) and iridium(III) (**3**) complexes derived from the azo-functionalized ligand (HL) and their comprehensive spectroscopic characterization including single-crystal X-ray structures. To the best of our knowledge this is the first report where CO generation through metal-assisted alcohol dehydrogenation in Ru(II)-2-(arylazo)phenol complex has been established using isotopic labeling, and along with that, a suitable mechanism has been proposed to understand the formation of the carbonyl-coordinated bivalent ruthenium complex **1**. In addition, the synthesized complexes were tested for their in vitro antiproliferative activity against human cervical (HeLa), human colorectal adenocarcinoma (HT-29), and mouse embryonic fibroblast (NIH-3T3) cell lines.

EXPERIMENTAL SECTION

General Methods and Materials. Chemicals were purchased from commercial sources and used without further purification. Ruthenium trichloride and iridium trichloride were obtained from Arora Matthey. $[Ru(PPh_3)_3Cl_2]$[28] and $[Ir(PPh_3)_3Cl]$[13a] were synthesized according to a previously reported procedure. Reagent-grade solvents were dried and distilled prior to use. $CH_3{}^{13}CH_2OH$ (99 atom % ^{13}C) was purchased from Sigma-Aldrich and used as received. Dulbecco's Modified Eagle Media (DMEM), Dulbecco's phosphate buffer saline (DPBS), trypsin ethylenediaminetetraacetic acid (EDTA) solution, fetal bovine serum (FBS), antibiotic-antimitotic solution, and 3-(4,5-dimethylthiazol-2-yl)-2,5-diphenyltetrazolium bromide (MTT) assay kit were purchased from Himedia. Tetramethylrhodamine B isothiocyanate (TRITC)-phalloidin and 4′,6-diamidino-2-phenylindole (DAPI) were procured from Sigma-Aldrich. HeLa and HT-29 cell lines were procured from NCCS. Elemental analyses were performed on a Vario ELcube CHNS Elemental analyzer. IR spectra were recorded on a PerkinElmer Spectrum RXI spectrophotometer. Attenuated total reflectance infrared (ATR-IR) spectra were recorded on a Bruker Tensor 27 ATR-FT-IR. ^{1}H, ^{13}C, and ^{31}P NMR spectra were recorded on a Bruker Ultrashield 400 MHz spectrometer using $SiMe_4$ as an internal standard. Electronic spectra were recorded on a Lamda25, PerkinElmer spectrophotometer. Mass spectra were obtained on an SQ-300 MS instrument operating in positive ion electrospray ionization (ESI) mode. High-resolution (HR) ESI mass spectrometry (MS) data were acquired using a Synapt G2-S HDMS instrument. A CH-Instruments (model CHI6003E) electrochemical analyzer was used for cyclic voltammetric experiments with CH_3CN solutions of the complexes containing tetrabutylammonium perchlorate (TBAP) as the supporting electrolyte. The three electrode measurements were performed at 298 K with a platinum working electrode, platinum auxiliary electrode, and saturated calomel electrode (SCE) as a reference electrode. ***Caution!*** *Although no problems were encountered during the course of this work, attention is drawn to the potentially explosive nature of perchlorates.*

Synthesis of the Ligand Precursor (HL). The azo ligand, 2-{2-(benzo[1,3]dioxol-5-yl)- diazo}-4-methylphenol (HL), was prepared as follows: 3,4-(methylenedioxy)aniline (2.74 g, 0.02 mol) was dissolved in 1:1 HCl/H_2O (37%, 30 mL). The solution was diazotized with $NaNO_2$ (1.4 g, 0.04 mol) in water (10 mL) at 0 °C. Separately *p*-cresol (2.25g, 0.04 mol) was dissolved in 10% NaOH

https://dx.doi.org/10.1021/acs.inorgchem.0c02563
Inorg. Chem. XXXX, XXX, XXX−XXX

Table 1. Crystal and Refinement Data of 1−3

complex	1•CH_3CN	2	3
empirical formula	$C_{53}H_{42}N_3O_4P_2Ru$	$C_{52}H_{43}N_3O_3P_2Ru$	$C_{50}H_{41}IrN_2O_3P_2$
formula weight	947.90	920.90	971.99
temperature	293(2) K	297(2) K	297(2) K
radiation	Mo Kα	Mo Kα	Mo Kα
crystal system	monoclinic	monoclinic	triclinic
space group	*Cm*	$P2_1/n$	$P\bar{1}$
unit cell dimensions	a = 18.2828(2) Å	a = 12.0619(2) Å	a = 11.1808(2) Å
	b = 14.6228(2) Å	b = 17.3951(2) Å	b = 12.0131(3) Å
	c = 9.68930(10) Å	c = 20.5496(3) Å	c = 19.2103(4) Å
	α = 90°	α = 90°	α = 101.2930(7)°
	β = 120.7910(4)°	β = 96.0240(6)°	β = 90.9690(7)°
	γ = 90°	γ = 90°	γ = 111.4660(6)°
volume	2225.25(5) Å^3	4287.87(11) Å^3	2343.66(9) Å^3
Z	2	4	2
density (calculated)	1.415 g/cm^3	1.427 g/cm^3	1.377 g/cm^3
absorption coefficient	0.475 mm^{-1}	0.489 mm^{-1}	2.958 mm^{-1}
F(000)	974	1896	972
crystal size	0.250 × 0.350 × 0.600 mm	0.025 × 0.100 × 0.200 mm	0.050 × 0.080 × 0.150 mm
θ range for data collection	1.90 to 28.34°	1.876 to 28.346°	1.95 to 30.77°
reflections collected	32 606	104 119	71 547
reflections unique	5305	10 676	14 045
final R1/wR2 [$I > 2\sigma(I)$]	R1 = 0.0233, wR2 = 0.0550	R1 = 0.0456, wR2 = 0.0954	R1 = 0.0319, wR2 = 0.0991

solution (15 mL), and the solution was cooled to 0 °C. The diazotized solution was then added slowly to the alkaline solution of *p*-cresol with continuous stirring at a temperature below 5 °C, until a greenish-red precipitate was obtained over a period of ∼30 min.[29]

The resulting greenish-red compound was filtered, washed with water, and dried over anhydrous $CaCl_2$. The purified ligand was obtained by slow evaporation of the saturated ethanolic solution of the crude product. Elemental analysis, NMR (^{1}H and ^{13}C), and IR data of the ligand confirmed its structure.

HL: Anal. Calcd for $C_{14}H_{12}N_2O_3$: C, 65.62; H, 4.72; N, 10.93. Found: C, 65.64; H, 4.70; N, 10.92%. Selected IR peaks with proposed assignments (KBr, ν_{max}/cm^{-1}): 3542 ν(O−H)$_b$, 1549 ν(N═N). ^{1}H NMR (400 MHz, $CDCl_3$): δ/ppm = δ 12.56 (s, 1H, −OH), 7.70−6.06 (m, 6H, aromatic), 4.23 (s, 2H, −O−CH_2−O), 2.39 (s, 3H, −CH_3). ^{13}C NMR (100 MHz, $CDCl_3$): δ/ppm = 153.60−115.88 (12C, aromatic), 101.02 (−O−CH_2−O), 24.30 (−CH_3). Yield: 4.096 g (16 mmol, 80%).

Synthesis of Ru(II) Complexes ([RuL(PPh$_3$)$_2$(CO)] (1), [RuL(PPh$_3$)$_2$(^{13}CO)] (1A), [RuL(PPh$_3$)$_2$(CH$_3$CN)] (2), and Ir(III) complex [IrL(PPh$_3$)$_2$(H)] (3). *[RuL(PPh$_3$)$_2$(CO)] (1).* 2-{2-(Benzo[1,3]-dioxol-5-yl)- diazo}-4-methylphenol (HL, 25.6 mg, 0.1 mmol) was dissolved in ethanol (EtOH, 50 mL) and refluxed for 10 min, followed by addition of triethylamine (22 mg, 0.22 mmol) and [$Ru(PPh_3)_3Cl_2$] (100 mg, 0.1 mmol). The resulting solution was refluxed in a nitrogen atmosphere for 24 h to yield a brown solution. The solvent was removed by rotary evaporation, and the solid mass, thus obtained, was subjected to purification by thin-layer chromatography on a silica plate. With 10:1.5 benzene-acetonitrile as the eluent, a prominent dark green band separated, which was extracted separately with acetonitrile. Evaporation of the acetonitrile extracts gave [RuL(PPh$_3$)$_2$(CO)] (**1**) as a green crystalline solid, from which single crystals suitable for X-ray diffraction could be picked. **1** could also be synthesized by an alternative procedure as mentioned below. **1A** was synthesized under identical experimental conditions, using isotopically labeled ethanol as solvent.

[RuL(PPh$_3$)$_2$CO] (1). Anal. Calcd for $C_{53}H_{42}N_3O_4P_2Ru$ (We calculated the formulation, considering the solvent molecule, CH_3CN, which is found as the solvent of crystallization during X-ray crystallography): C, 66.30; H, 4.58; N, 4.55. Found: C, 66.36; H, 4.53; N, 4.61. Main IR peaks (KBr, υ_{max}/cm^{-1}): 1936 υ(CO); 1478 υ(N═N); 1238 ν(C−O)$_{phenolic}$; 750, 691, 519 υ(3P−Ph). ^{1}H NMR (deuterated dimethyl sulfoxide (DMSO-d_6), 400 MHz) δ (ppm): 7.65−7.24 (2PPh$_3$); 6.99−5.97 and 5.80 (m, 5H, Ar−H); 5.89 (s, 2H, O−CH_2−O); 1.75 (s, 3H, ArCH_3). ^{31}P NMR δ (ppm): 33.97. Yield: 42 mg (44.31 μmol, 45%).

[RuL(PPh$_3$)$_2$(CO)] (1) and [RuL(PPh$_3$)$_2$(^{13}CO)] (1A). A 10 mL microwave tube was charged with 2-{2-(benzo[1,3]dioxol-5-yl)-diazo}-4-methylphenol (5.0 mg, 19.5 μmol) and [$Ru(PPh_3)_3Cl_2$] (18.71 mg, 19.5 μmol). Ethanol (or ethanol-1-^{13}C, 0.50 mL) and triethylamine (0.15 mL) were then added, and the tube was quickly flushed with N_2 (g) and sealed. The mixture was then sonicated for 5 min to form a brown suspension, then subjected to microwave irradiation for 1 h (T = 130 °C, P = 90 W). After it cooled to ambient temperature, a green solution was obtained. This solution was then taken to dryness at reduced pressure to give a green solid, which was dissolved in ethyl acetate (EtOAc) (1 mL) and filtered to remove colorless and brown impurities before being loaded onto silica and purified by column chromatography using a Combiflash Rf system (gradient 0 → 5% EtOAc in hexane, rf (5% EtOAc) = 0.1). The dark green product containing fraction was taken to dryness at reduced pressure to give pure [RuL(PPh$_3$)$_2$(CO)], **1** (or [RuL(PPh$_3$)$_2$-(^{13}CO)], **1A**) as a dark green solid. Yield: 4.5 mg (4.96 μmol, 25.4%).

[RuL(PPh$_3$)$_2$(CH$_3$CN)] (2). This complex was prepared essentially by the same procedure used for the synthesis of **1**, except that acetonitrile was used as the solvent instead of ethanol. The brown solution obtained in this case was dried. The solid mass obtained, upon rotary evaporation, was subjected to purification by thin-layer chromatography on a silica plate. With 10:1.5 benzene−acetonitrile as the eluent, the major brown colored fraction was separated. The isolated fraction was extracted with acetonitrile. Brown crystals of **2** were obtained upon slow evaporation of the extract.

[RuL(PPh$_3$)$_2$(CH$_3$CN)] (2). Anal. Calcd for $C_{52}H_{43}N_3O_3P_2Ru$: C, 67.82; H, 4.71; N, 4.56. Found: C, 67.78; H, 4.73; N, 4.51%. Main IR peaks (KBr, υ/cm^{-1}): 2212 υ(CH_3CN); 1487 υ(N═N); 1245 υ(C−O)$_{phenolic}$; 749, 690, 516 υ(3P−Ph). ^{1}H NMR (DMSO-d_6,400 MHz) δ (ppm): 7.65−5.78 (m, 35H, Ar−H and PPh_3); 5.89 (s, 2H, O−CH_2−O); 2.51 (s, 3H, CH_3CN); 1.75 (s, 3H, ArCH_3). ^{31}P NMR, δ (ppm): 33.93. Yield: 44 mg (47.78 μmol, 48%).

[IrL(PPh$_3$)$_2$(H)] (3). 2-{2-(Benzo[1,3]dioxol-5-yl)-diazo}-4-methylphenol (25.6 mg, 0.1 mmol) was dissolved in ethanol (50 mL) and refluxed for 10 min, followed by addition of triethylamine (22 mg, 0.22 mol) and [$Ir(PPh_3)_3Cl$] (100 mg, 0.1 mmol). The resulting solution was refluxed under a nitrogen atmosphere for 32 h to yield a

https://dx.doi.org/10.1021/acs.inorgchem.0c02563
Inorg. Chem. XXXX, XXX, XXX−XXX

Scheme 1. Schematic Diagram for the Syntheses of $[RuL(PPh_3)_2(CO)]$ (1), $[RuL(PPh_3)_2(CH_3CN)]$ (2), and $[IrL(PPh_3)_2(H)]$ (3)

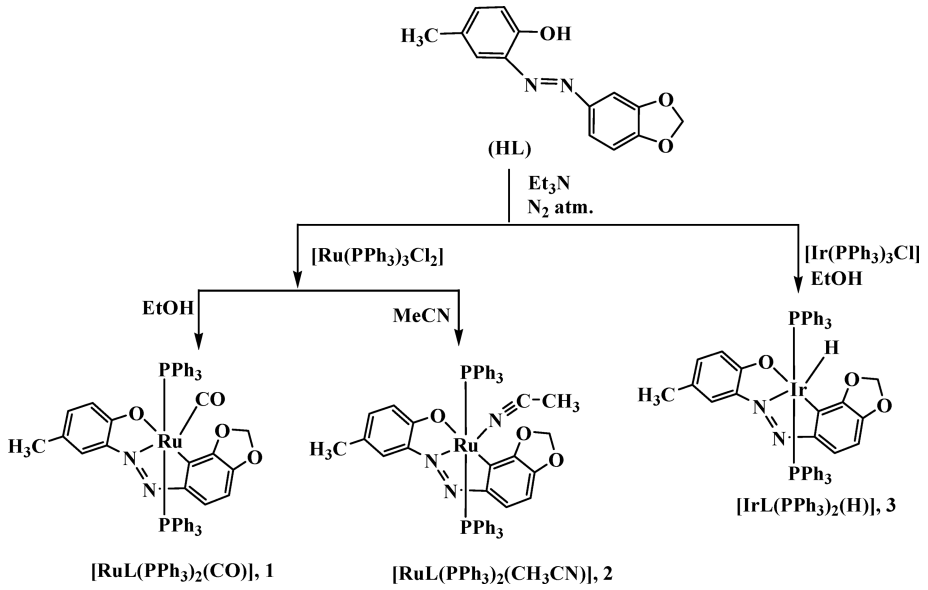

green solution. The solvent was removed by rotary evaporation, and the resulting solid mass was subjected to purification by thin-layer chromatography on a silica plate. With 1:1 benzene−toluene as the eluent, a dark blue band separated, and the corresponding material was extracted separately with acetonitrile. Blue crystals of $[IrL(PPh_3)_2(H)]$ (**3**) were obtained by the slow evaporation of the acetonitrile extract over a period of three weeks.

*[IrL(PPh$_3$)$_2$(H)] (**3**).* Anal. Calcd for $C_{50}H_{41}IrN_2O_3P_2$: C, 61.78; H, 4.25; N, 2.88. Found: C, 61.73; H, 4.20; N, 2.93%. Main IR peaks (KBr, υ/cm^{-1}): 2050 υ(Ir−H); 1480 υ(N═N); 1237 $\upsilon(C-O)_{phenolic}$; 746, 694, 515 υ(3P−Ph). ^{1}H NMR (DMSO-d_6,400 MHz) δ (ppm): 7.36−7.23 (m, 15H, PPh_3); 6.79−5.95 (m, 5H, Ar−H); 5.68 ppm (s, 2H, O−CH_2−O); 1.88 (s, 3H, $ArCH_3$); −12.54 (t, hydride, Ir−H). ^{31}P NMR, δ (ppm): 11.90, 9.89. Yield: 43.7 mg (44.95 μmol, 45%).

X-ray Crystallography. Single crystals of the complexes were mounted on a Bruker Smart ApexII single-crystal diffractometer equipped with a graphite monochromator and a Mo Kα X-ray source (λ = 0.710 73 Å). Crystallographic data and the details of refinement are given in Table 1. Unit cell dimensions and intensity data were measured at 293(2) K for **1** and 297(2) K for **2** and **3**. Integrated intensities were obtained with the Bruker SAINT[30] software package using a narrow frame logarithm. The intensity data were corrected for Lorentz, polarization, and absorption effects. Absorption corrections were applied using SADABS,[31] and the structures were solved by direct methods using the program SHELXS[32] and refined using least-squares with the SHELXL[32] software program. Hydrogen atoms were either found or placed in calculated positions and isotropically refined using a riding model. The non-hydrogen atoms were refined anisotropically. Figures were drawn using DIAMOND and MERCURY. In the ball-and-stick models all atoms are drawn as thermal displacement ellipsoids of the 40% level with exception of the hydrogen atoms, which are shown as spheres of arbitrary radii. Complex **3** contained disordered solvent that could not be refined explicitly. The contribution of the solvent electron density to the diffraction data was removed via SQUEEZE.

Cytotoxicity. The in vitro cytotoxicity of the complexes was explored against human cervical cancer (HeLa), colon cancer (HT-29), and noncancerous mouse embryonic fibroblast (NIH-3T3) cells. In a typical procedure, cells were cultured in DMEM media containing 10% FBS under a humidified 5% CO_2 incubator at 37 °C. During the experiment cells at a concentration of 8×10^3 cells/well were seeded in a 96-well culture plate and kept in the incubator. After 12 h of seeding, complexes **1**−**3** in the concentration range of 5−100 μg/mL were added to the cells for a period of 48 h. The complexes were initially dissolved in DMSO at a concentration of 3 mg/mL and then diluted in media to achieve the desired concentration. Cells cultured in media alone were taken for the control experiment. Subsequently, after the treatment period, the used media were removed, and the cells were treated with MTT over an additional period of 4 h. Later from each well the MTT-containing media was removed, and 200 μL of DMSO was added. After 30 min of incubation in dark the optical density was measured using a microplate reader spectrophotometer at 595 nm. The experiment was performed in quadruplets, and the data were expressed as mean ± standard deviation (SD). Single variance analysis of variance (ANOVA) under 95% confidence interval was used to evaluate the statistical significance of the data.

$$\%\text{cell viability} = [\text{mean OD of the treated cell} / \text{mean OD of the control}] \times 100 \quad (1)$$

Analysis of Nuclear Morphology with Hoechst Staining. The nuclear morphology of the cancer cells in the presence of the test complexes was examined with a DNA binding fluorescence dye, namely, Hoechst. For this study, cells were incubated with half-maximal inhibitory concentration (IC_{50}) of the complexes for 12 h in confocal dishes. The cells were then washed gently with PBS, fixed with 4% paraformaldehyde for 15 min, and permeabilized (using 0.25% Triton X-100 in PBS, 10 min exposure). Postpermeabilization cells were stained with Hoechest (for nucleus staining), and the image was recorded under confocal microscopy (Leica, SP8).[33]

RESULTS AND DISCUSSION

Synthesis and Characterization. The reaction of an equimolar mixture of 2-(arylazo)phenol, HL, with $[Ru(PPh_3)_3Cl_2]$ in refluxing ethanol or acetonitrile under basic conditions in a nitrogen atmosphere afforded two distinct products with different colors, specifically, green and brown, which were shown to have the stoichiometry $[RuL(PPh_3)_2(CO)]$ (**1**) and $[RuL(PPh_3)_2(CH_3CN)]$ (**2**), respectively. The reaction of HL with $[Ir(PPh_3)_3Cl]$ under the same conditions, however, resulted in the formation of blue crystals of $[IrL(PPh_3)_2(H)]$ (**3**). The synthetic methodology of **1**−**3** is illustrated in Scheme 1. Elemental analyses, IR and NMR spectra, and ESI-MS of **1**−**3** allowed for a thorough initial characterization of the complexes, which was confirmed by X-

https://dx.doi.org/10.1021/acs.inorgchem.0c02563
Inorg. Chem. XXXX, XXX, XXX−XXX

Scheme 2. Proposed Mechanisms[a]

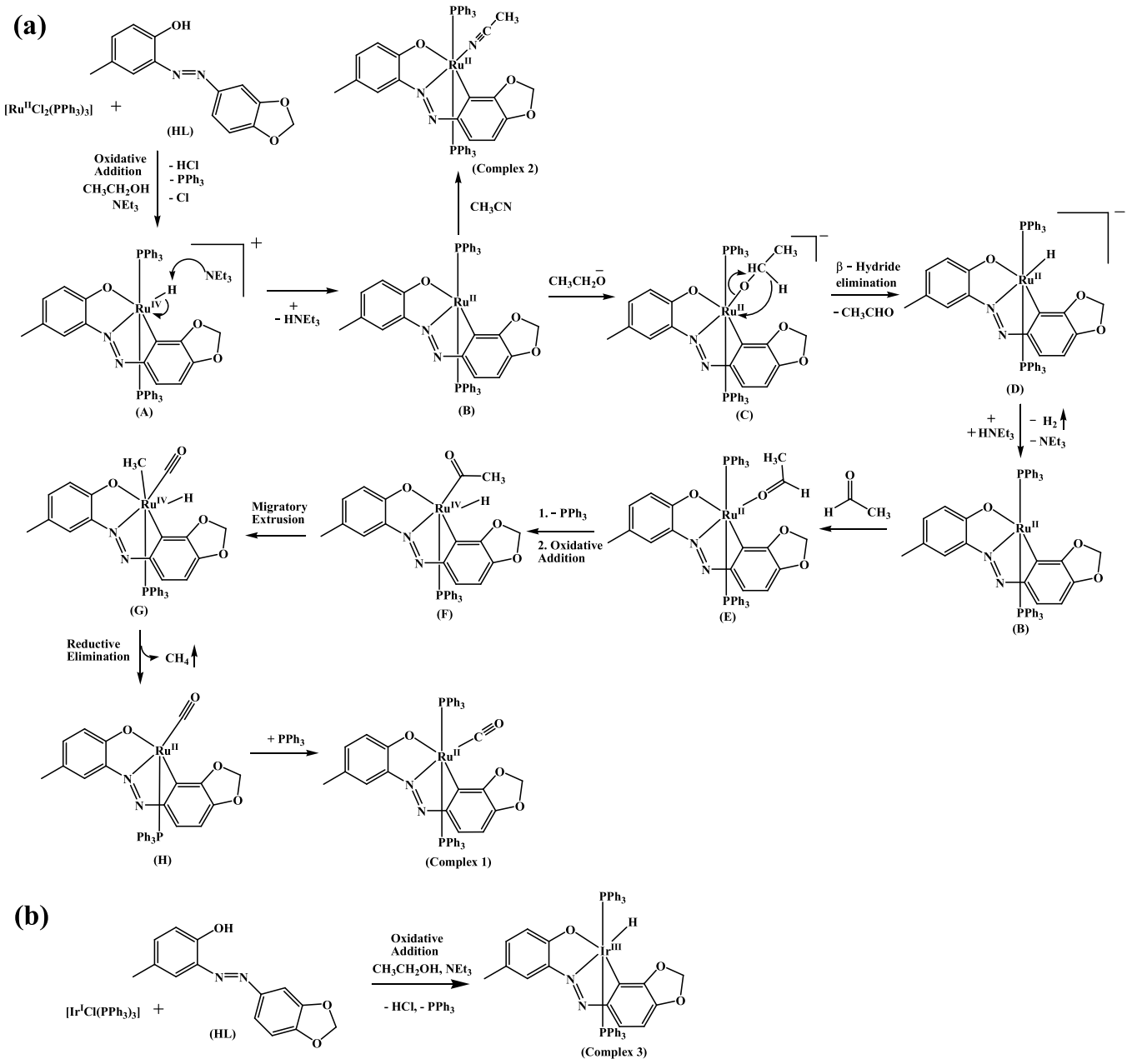

[a]Proposed mechanisms for the formation of (a) $[RuL(PPh_3)_2(CO)]$ (**1**) and $[RuL(PPh_3)_2(CH_3CN)]$ (**2**) and (b) $[IrL(PPh_3)_2(H)]$ (**3**).

ray crystallography. The complexes were slightly soluble in ethanol and methanol but completely soluble in other protic and aprotic solvents. The time-dependent solution stability of **1** and **3** was investigated by electronic absorption spectral studies over a period of 48 h in a mixture of both DMSO and DPBS solution (Figures S1 and S2) and DMSO and DMEM solution (Figures S1 and S2), which showed the complexes are stable in these solvent mixtures for at least 48 h.

The ligand coordinates to the metal center in the case of all the three complexes as a tridentate C, N, O-donor via metal-assisted C−H activation, which is well-documented in the literature.[10,13a,34−36] In the case of $[RuL(PPh_3)_2(CH_3CN)]$ (**2**), the acetonitrile used as the reaction solvent coordinates to the Ru center at the sixth coordination site, while the hydride generated from C−H activation of the ligand coordinates at the sixth coordination site in $[IrL(PPh_3)_2(H)]$ (**3**). However, the coordination of a carbonyl group to the Ru(II) center in the case of $[RuL(PPh_3)_2(CO)]$ (**1**) was unexpected, since the metal precursor, $[Ru(PPh_3)_3Cl_2]$, used for synthesis of **1** cannot serve as a source of CO. The earlier report of Acharyya et al. on unexpected CO coordination in arylazo ruthenium(II) complexes in ethanolic medium attributed the CO formation to the migration of an alkyl group in the ligand backbone and its subsequent oxidation to CO, resulting in ligand modification.[10] However, in the case of complex **1**, a similar explanation was not possible, since the substituted methyl group in the ligand remained intact even after complex formation. The formation of Ru−CO complexes, by heating Ru(II) and Ru(III) compounds in the presence of primary alcohols, has earlier been established by Yi et al.[37] and Jayanthi

https://dx.doi.org/10.1021/acs.inorgchem.0c02563
Inorg. Chem. XXXX, XXX, XXX−XXX

et al.,[11] without mechanistic details however. Taking these literature reports into consideration, the source of CO was assumed to be the solvent (ethanol) used for synthesis. To test this hypothesis, the reaction of HL with $[Ru(PPh_3)_3Cl_2]$ was performed in toluene and acetonitrile, in basic medium. Indeed, preliminary characterization (IR) of the products obtained from toluene and acetonitrile did not show any trace of CO generation in the reaction medium, thereby suggesting that EtOH is the source of CO. We also experimentally performed the synthesis and spectroscopic characterization of complex **1** in methanol and isopropyl alcohol solvent media. The characteristic sharp peak of CO is clearly observed in the case of the complex isolated from methanol and isopropyl alcohol as the solvent (Figure S3). To gain further support for the generation of CO via ruthenium-assisted ethanol oxidation, as in complex **1**, the synthesis was repeated using ethanol-1-^{13}C, which resulted in the incorporation of a ^{13}C-labeled carbonyl group into the product. This was confirmed by IR spectroscopy and ESI-MS. Chakravorty et al. previously reported the synthesis of Os and Ru complexes, wherein decarbonylation of a diformylphenol Schiff base ligand had occurred resulting in the formation of CO coordinated to the organometallic complexes.[38] In their case however the CO coordination was indifferent to variations of the solvent. On the basis of the above discussion, a mechanistic scheme for the formation of **1** is proposed in Scheme 2a. Simultaneously, a probable pathway for the formation of **2** and **3** is also shown in Scheme 2a,b, respectively.

In the first step of Scheme 2a, the metal precursor $[RuCl_2(PPh_3)_2]$ reacts with HL in the presence of NEt_3 forming complex **A** by deprotonation of the phenolic O−H and C−H activation of HL, thereby resulting in loss of PPh_3 and HCl. The fourth equatorial site in **A** is occupied by the hydride ligand, resulting in the formation of a Ru(IV) cationic complex **A**. This is in line with the C−H oxidative addition that we observe for the formation of the Ir(III) complex **3** (Scheme 2b). Ir(III) complex (**3**), once formed after oxidative addition, attains a stable 18-electron configuration, so further reaction does not take place. The stability of the +III oxidation state of the iridium center explains the inertness of complex **3** toward CO generation. However, the comparatively unstable 16-electron species formed in the case of Ru (intermediate **A** in Scheme 2a) can react further to attain stability. Compound **A** is deprotonated, for example, by triethylamine, to form the Ru(II) species **B**, which is a key reactive 16-electron intermediate. This reactive 16-electron intermediate **B** can be trapped by a coordinating solvent such as CH_3CN, if present (as in the formation of complex **2**). If no such strongly coordinating solvent is present, the ethoxide ion (formed upon deprotonation of ethanol in basic medium) coordinates to the coordinatively unsaturated Ru(II) center of **B**, forming **C**. The resulting complex **C** undergoes β-hydride elimination, giving one molecule of CH_3CHO through alcohol dehydrogenation and simultaneous coordination of a hydride ion to the ruthenium center to form **D**. In the next step, the coordinatively unsaturated Ru(II) complex **B** is again formed via deprotonation. The aldehyde CH_3CHO generated previously in the reaction coordinates to the metal center to form **E**. In the next step, the resulting complex **E** loses PPh_3 and undergoes oxidative addition forming the Ru(IV) species **F**. This is followed by a migratory extrusion to form the Ru(IV) complex (**G**) and then reductive elimination with the loss of methane. Finally, addition of PPh_3 to the unsaturated species **H** results in the formation of the product complex **1** (Scheme 2a).[38b,39,40]

Spectral Characteristics. *IR Spectroscopy.* A broad band at ∼3450 cm^{-1} was observed for HL, due to the presence of OH group, which disappears upon the formation of **1**−**3**. The IR stretching frequency of HL observed at 1549 cm^{-1} is attributed to the presence of the azo(N═N) functional group.[41] The corresponding peak shifts to a lower frequency range of ∼1481 cm^{-1} upon complexation (**1**−**3**). The presence of a coordinated CO in the case of **1** is evident from the characteristic peak of CO, observed at 1936 cm^{-1},[10] while an extra peak at 2212 cm^{-1} in the IR spectra of **2**, as compared to the ligand, could be attributed to the CN stretching frequency in the complex. Besides the difference in the CO and CN stretch, the infrared spectra of **1** and **2** are very similar. The presence of three strong absorption bands (∼515, 694, and 746 cm^{-1}) in **1**, **2**, and **3** is due to the coordinated PPh_3 ligands, and the peak at 2050 cm^{-1} is assigned to the Ir−H stretching frequency.[34c] In the ^{13}C-labeled carbonyl Ru(II) complex (**1A**) the CO stretching band is shifted by 49 cm^{-1} to lower frequency due to the presence of the heavier carbon isotope. The remaining IR bands are mostly unaffected (Figure 1). The reason for the weak band at 1932 cm^{-1} in the IR

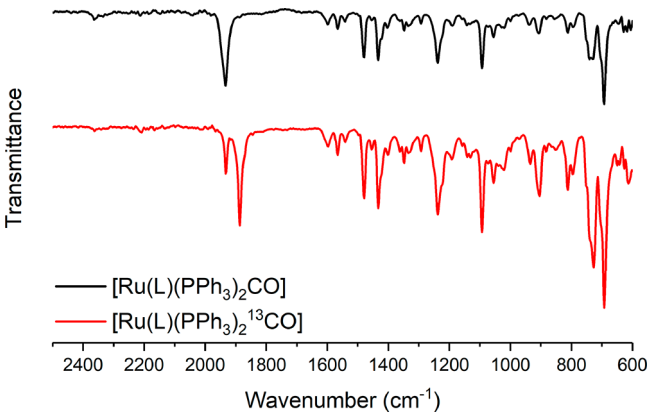

Figure 1. ATR-IR spectrum of $[Ru(L)(PPh_3)_2(CO)]$ (**1**, top) and $[Ru(L)(PPh_3)_2(^{13}CO)]$ (**1A**, bottom).

spectrum of the labeled product is unclear. However, a possible explanation is the formation of a small amount of ^{12}CO, which might have been generated from unlabeled ethanol still present in $[Ru(PPh_3)_3Cl_2]$ or ligand (HL). A comparison of the ATR-IR spectra of $[Ru(L)(PPh_3)_2(CO)]$ (**1**) and $[Ru(L)(PPh_3)_2(^{13}CO)]$ (**1A**) is shown in Figure 1, while the Fourier transform infrared (FT-IR) spectrum of **3** is shown in Figure 2.

ESI-MS. The ESI-MS of **1**−**3** were recorded in acetonitrile solution. The ESI-MS of **1** shows the molecular ion peak $[M]^+$ at m/z = 907.90, whereas the ESI-MS for **2** and **3** display molecular ion peaks, $[M]^+$, at m/z = 921.10 and 972.77, respectively. The incorporation of the labeled carbon atom was further confirmed by ESI-MS and HR-ESI-MS, whereby the signal from the molecular ion as well as from the other fragments that contain the carbonyl are all shifted by one m/z unit. Figures 3 and 4 represent the HR-ESI-MS spectra of **1** and **1A** respectively, while Figures S4−S6 depict the representative ESI-MS spectra of **1**, **1A**, and **3**, respectively.

UV−Vis spectroscopy. The electronic spectra of $[RuL(PPh_3)_2(CO)]$ (**1**), $[RuL(PPh_3)_2(CH_3CN)]$ (**2**), and $[IrL(PPh_3)_2(H)]$ (**3**) were recorded in dichloromethane solution.

https://dx.doi.org/10.1021/acs.inorgchem.0c02563
Inorg. Chem. XXXX, XXX, XXX−XXX

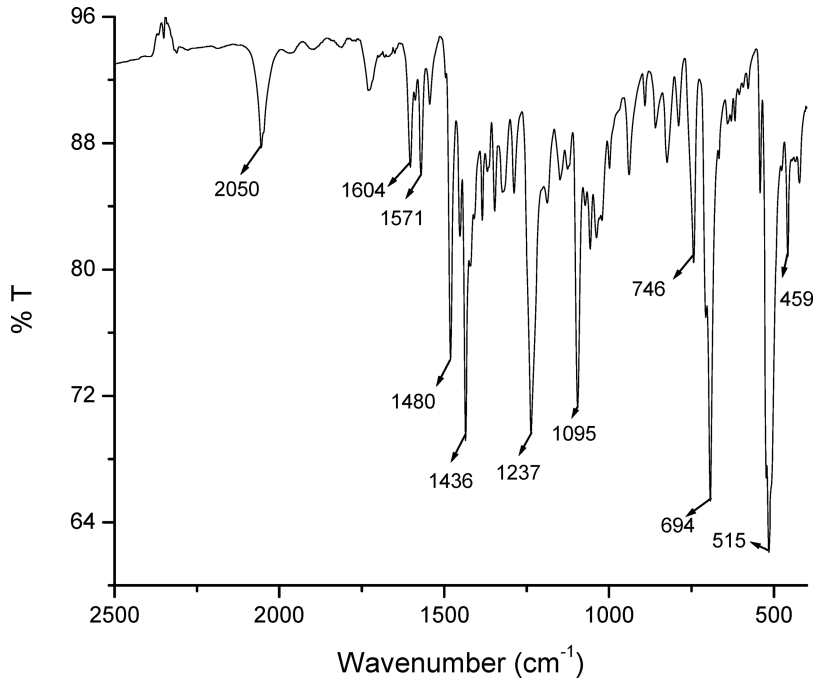

Figure 2. FT-IR spectrum of $[IrL(PPh_3)_2(H)]$ (**3**).

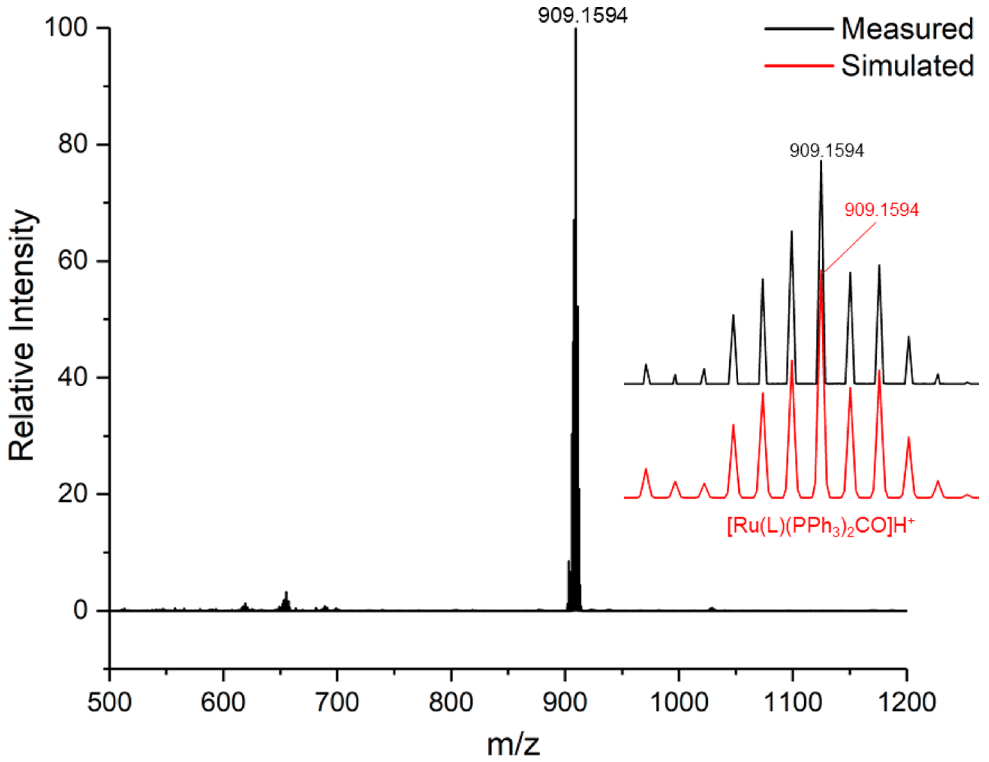

Figure 3. HR-ESI-MS spectrum of $[Ru(L)(PPh_3)_2(CO)]$ (**1**).

The strong transitions in the UV region of **1**, **2**, and **3** are attributable to intraligand charge transfer transitions, whereas the weaker absorptions in the lower-energy region of the spectra are presumably due to metal-to-ligand charge transfer transition (MLCT).[42,43] Representative UV−vis spectra of **1** and **3** are shown in Figure S7, and the values are tabulated in Table 2.

NMR Spectroscopy. ^{1}H NMR spectra of all complexes were recorded in DMSO-d_6. The NMR spectral data of **1**−**3** are in agreement with their respective composition and stereochemistry. The ^{1}H NMR spectra of **1** and **2** are qualitatively similar. An extra three-proton singlet is observed in **2** due to the methyl group of the coordinated CH_3CN. The ^{1}H NMR spectrum of complex **3** shows a hydride signal as a distinct triplet due to coupling with two magnetically equivalent phosphorus nuclei, near ca. −12.54 ppm. A detailed discussion of the ^{1}H NMR is provided in the Supporting Information.

https://dx.doi.org/10.1021/acs.inorgchem.0c02563
Inorg. Chem. XXXX, XXX, XXX−XXX

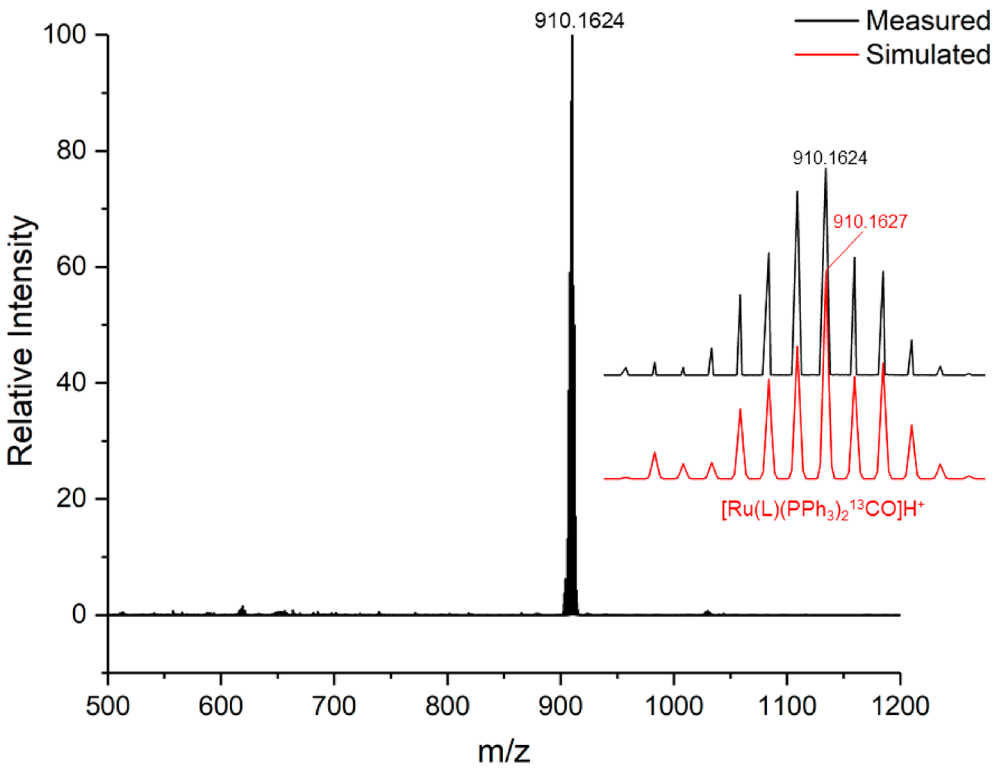

Figure 4. HR-ESI-MS spectrum of $[Ru(L)(PPh_3)_2(^{13}CO)]$ (**1A**).

Table 2. Electronic Spectra for Complexes 1−3 in Dichloromethane Solution

complex	λ_{max}/nm (ϵ_{max}/M^{-1} cm^{-1})
$[RuL(PPh_3)_2(CO)]$ (**1**)	207 (26 533), 224 (16 000), 262 (5000), 348 (1666), 449 (1333), 642 (1200)
$[RuL(PPh_3)_2(CH_3CN)]$ (**2**)	278 (45 121), 230 (25 000), 258 (8500), 385 (27 637), 457 (9500), 668 (1400)
$[IrL(PPh_3)_2(H)]$ (**3**)	210 (26 666), 258 (10 133), 336 (2333), 433 (1466), 598 (2533)

Representative ^1H spectra of **1** and **3** are given in Figures S8 and S9, respectively.

Electrochemical Properties. The potential data of **1**−**3** are tabulated in Table S1, and the representative cyclic voltammograms of **1**, **3**, and ligand (HL) are given in Figures S10−S12, respectively. The cyclic voltammogram patterns of **1** and **2** are similar; each exhibits a single electron transfer quasi-reversible oxidative wave Ru(II)/Ru(III)[14b,c,34a] in the anodic region at $E^a_{1/2}$ value of +0.54 and +0.52 V, respectively, while **3** shows a reversible redox couple for Ir(III)/Ir(IV)[13a,34c,36] at +0.50 V. An irreversible ligand-centered oxidation and reduction peak is observed at +1.25 and −1.4 V in the anodic and cathodic region, respectively.[13a,34c,36] The one-electron nature of this oxidation was verified by comparing its current height with that of the standard ferrocene−ferrocenium couple under identical experimental conditions.

Description of the X-ray Structure of [RuL(PPh$_3$)$_2$CO] (1), [RuL(PPh$_3$)$_2$(CH$_3$CN)] (2), and [IrL(PPh$_3$)$_2$(H)] (3). $[RuL(PPh_3)_2CO]$ (**1**): The molecular structure and the atom numbering scheme for $[RuL(PPh_3)_2CO]$ (**1**) is shown in Figure 5, and the relevant bond parameters are collected in Table 3. The structure of **1** shows that the 2-(arylazo)phenol ligand is coordinated to the metal (via loss of the phenolic proton as well as another proton from one ortho position of

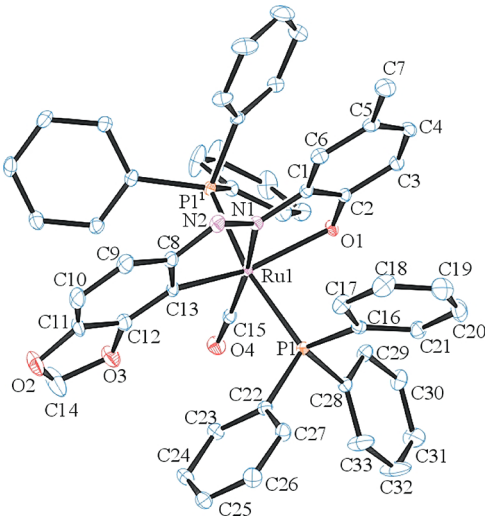

Figure 5. ORTEP diagram of the asymmetric unit of $[RuL(PPh_3)_2CO]$ (**1**). H atoms and acetonitrile molecule of solvation were omitted for clarity, and thermal ellipsoids are shown at 40% probability.

the phenyl ring in the arylazo fragment) as a tridentate C, N, O-donor, resulting in a distorted octahedral coordination geometry of **1**. The remaining three coordination sites are occupied by two triphenylphosphines and a carbon monoxide molecule. The coordinated 2-(arylazo)phenolate ligand and CO share an equatorial plane with Ru at the center, where the CO is trans to the coordinated azo-nitrogen(N1). Perfect planarity of the arylazo ligand is enforced by a mirror plane, and this also forces the PPh_3 ligands, which occupy the axial positions (P−Ru−P angle is 167.4°), to be mirror-images. Both Ru−PPh_3 distances are hence identical [Ru(1)−P(1) =

https://dx.doi.org/10.1021/acs.inorgchem.0c02563
Inorg. Chem. XXXX, XXX, XXX−XXX

Table 3. Selected Geometric Parameters for Complexes 1–3[a]

bond distances (Å)	1	2	3
M–N(1)	2.045(3)	1.989(2)	2.033(2)
M–O(1)	2.195(3)	2.160(2)	2.180(2)
M–C(13)	2.042(5)	2.026(3)	2.023(2)
M–P(1)	2.3716(6)	2.3833(8)	2.3219(6)
M–P(2)	2.3716(6)	2.3641(8)	2.3142(6)
M–X	1.862(4)	1.997(3)	1.51(2)
bond angles (deg)			
C(13)–M–N(1)	76.9(2)	77.0(1)	77.91(8)
C(13)–M–O(1)	154.9(1)	156.4(1)	156.68(8)
X–M–O(1)	109.6(2)	99.3(1)	103.8(3)
X–M–C(13)	95.5(2)	104.3(1)	99.4(9)
X–M–N(1)	172.4(2)	178.7(1)	177.3(9)
X–M–P(1)	89.0(2)	88.43(9)	84.3(9)
X–M–P(2)		87.96(9)	84.0(9)
P(1)–M–P(2)	167.36(3)	176.38(3)	163.75(2)
N(1)–M–O(1)	77.9(1)	79.47(9)	78.88(7)
N(1)–M–P(1)	91.8(1)	91.64(7)	96.10(5)
C(13)–M–P(1)	96.3(1)	92.19(8)	97.50(6)
O(1)–M–P(1)	84.44(8)	89.73(6)	82.74(5)
N(1)–M–P(2)		91.98(7)	96.16(5)
C(13)–M–P(2)		88.43(8)	95.47(6)
O(1)–M–P(2)		91.14(6)	89.21(5)

[a]Selected geometric parameters, where M = Ru, complexes **1** and **2**; M = Ir, complex **3**; Ligand (X) = −CO [**1**], −$NCCH_3$ [**2**], −H [**3**]).

2.3716(6) Å] and comparable to those found in similar complexes.[34a] A CH_3CN molecule is also present as the solvent of crystallization in the crystal lattice of **1** (not shown in Figure 5 below).

$[RuL(PPh_3)_2(CH_3CN)]$ (**2**): The molecular structure and the atom numbering scheme for $[RuL(PPh_3)_2(CH_3CN)]$ (**2**) is shown in Figure 6, and the relevant bond parameters are tabulated in Table 3. The ligand is coordinated to the Ru center as a tridentate dianionic C, N, O donor as in the case of **1**. However, in **2**, the fourth coordination site in the equatorial plane is occupied by a CH_3CN group instead of CO. Two five-membered chelate rings define the equatorial plane with bite angles 77.0(1)° [C(13)–Ru(1)–N(1)] and 79.47(9)° [O(1)–Ru(1)–N(1)]. The two triphenylphosphines are located trans to each other in the axial plane, the bond angle P(1)–Ru(1)–P(2) being 176.38(3)°. In the case of $[RuL(PPh_3)_2(CH_3CN)]$ (**2**), there is a slight difference in the bond distance between Ru(1)–P(1) (2.3610(6) Å) and Ru(1)–P(2) (2.3834(8) Å), resulting in the formation of a distorted octahedral geometry, as compared to $[RuL(PPh_3)_2(CO)]$ (**1**), where both the Ru(1)–P(1) bonds are equidistant. Notably, the Ru(1)–N(1) distance (1.989(2) Å) in **2** is shortened as compared to the Ru(1)–N(1) distance (2.045(3) Å) of **1** due to the weaker trans effect of CH_3CN (in **3**) than CO (in **1**).

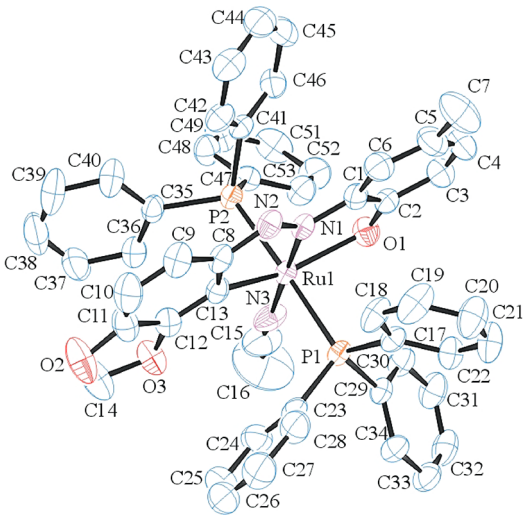

Figure 6. ORTEP diagram of $[RuL(PPh_3)_2(CH_3CN)]$ (**2**). H atoms were ommitted for clarity; thermal ellipsoids are shown at 40% probability.

$[IrL(PPh_3)_2(H)]$ (**3**): The structure of the Ir(III) complex $[IrL(PPh_3)_2H]$ (**3**) is illustrated in Figure 7, and selected bond parameters are also tabulated in Table 3. While the overall appearance is an octahedral complex, the bond parameters reflect the distortion of the coordination geometry of the cyclometalated organometallic complex (**3**) from an ideal octahedron. The bond distances Ir(1)–C(1), Ir(1)–N(1), Ir(1)–O(1), Ir(1)–H(1), Ir(1)–P(1), and Ir(1)–P(2) within the C, N, O-chelated fragment of **3** are consistent with those of previous examples in the literature.[13a] The equatorial plane in the complex is defined by two five-membered rings formed by the coordination of the ligand as a tridentate C, N, O donor with bite angles of 77.91(8)° [C(1)–Ir(1)–N(1)] and 78.88(7)° [N(1)–Ir(1)–O(1)]. In addition, a hydride occupies the equatorial plane positioned trans to the N1 atom, while two PPh_3 groups occupy the axial positions in complex **3**.

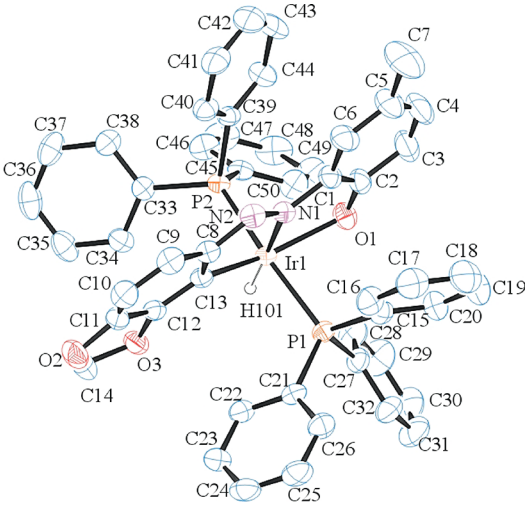

Figure 7. ORTEP diagram of $[IrL(PPh_3)_2(H)]$ (**3**). Solvent removed via SQUEEZE. Thermal ellipsoids are shown at 40% probability.

Cytotoxicity Studies. A number of ruthenium and iridium complexes have been reported to show cytotoxicity against cancer cells in vitro.[18b,c,44−47] Inspired by this, we evaluated the cytotoxicity of the Ru(II) and Ir(III) arylazo complexes against HeLa and HT-29 cell lines. Complexes **1**–**3** were shown to act as potent cytotoxic agents, whereas the ligand HL and metal precursors were inactive (IC_{50} > 100 μM). The IC_{50} values of the complexes are in the ranges of 3.8–4.2 and 3.3–4.5 μM for HeLa and HT-29 cells, respectively (Table 4). A plausible elucidation is that, by coordination, the polarity of the ligand and the central metal ion are reduced through the

https://dx.doi.org/10.1021/acs.inorgchem.0c02563
Inorg. Chem. XXXX, XXX, XXX−XXX

Table 4. Antiproliferative Effect of Complexes 1−3[a]

	IC_{50} (μM)		
complexes	HeLa cells	HT-29 cells	NIH-3T3
1	4.22 ± 0.11	4.34 ± 0.25	6.64 ± 0.18
2	3.84 ± 0.15	4.48 ± 0.25	7.24 ± 0.19
3	4.00 ± 0.20	3.27 ± 0.21	4.56 ± 0.17

[a]Antiproliferative effect against HeLa, HT-29, and NIH-3T3 cells. The IC_{50} values were determined by the MTT assay, after 48 h of incubation. The experiments were performed in quadruplicates, and IC_{50} values are reported as mean value ± standard deviation.

charge equilibration, which favors permeation of the complexes through the lipid layer of the cell membrane.[26a,48,49] Moreover, the higher activity can be attributed to the increased lipophilicity on chelation of the ligand to the metal center.[25b,50] A comparison of the IC_{50} values of **1**−**3** with a clinically used anticancer drug revealed that the antiproliferative activity of all metal complexes **1**−**3** is greater than that of cisplatin (12.2 and 70 μM) and comparable with that of other established drugs such as tamoxifen (9.3 and 8.82 μM) and 5-fluorouridine (0.3 and 2.85 μM) in HeLa and HT-29, respectively.[51]

The data in Table 4 and Figure 8 show that all three new metal complexes are highly potent, with only minimal differences between the metals or cancer cell lines. The high activity of Ru(II) complexes toward cervix carcinoma HeLa cancer cells in comparison to colon adenocarcinoma HT-29 has previously been observed with other Ru(II) systems (such as $[Ru(\eta^6\text{-}p\text{-cymene})(N\text{-MeIm})_3]Cl_2\cdot 2H_2O$ and $[Ru(\eta^6\text{-}p\text{-cymene})(N\text{-PrIm})Cl_2]$) bearing a different ligand backbone.[44] To have pharmacological applications, a potent anticancer drug needs to be specific for cancer cells, without many damaging effects on normal cells. Therefore, the cytotoxic effect of the present sets of complexes was also tested on noncancerous mouse embryonic fibroblast (NIH-3T3) cells. From the IC_{50} values, it was observed that the complexes were slightly less toxic to normal cells in comparison to cancer cells (Table 4, Figure 8). Overall, complex **2** with relatively higher cytotoxicity toward cancer cells in comparison to normal cells can be said to have exhibited the most encouraging result among the series.

Both the synthesized Ru(II) complexes (**1** and **2**) show lower IC_{50} values against HT-29 cancer cell lines compared to the Keppler-type Ru(III) anticancer complexes and their trifluoromethyl derivatives (IC_{50} > 100−24 μM).[45] The reported Ir(III) and Ru(II) azo complexes in the present study were also found to be more potent or comparable against HeLa cancer cells as compared to the zwitterionic, cationic hydrazone-functionalized complex (IC_{50} > 100−3.4 μM),[46] as well as naphthalimide-modified half-sandwich iridium(III) and

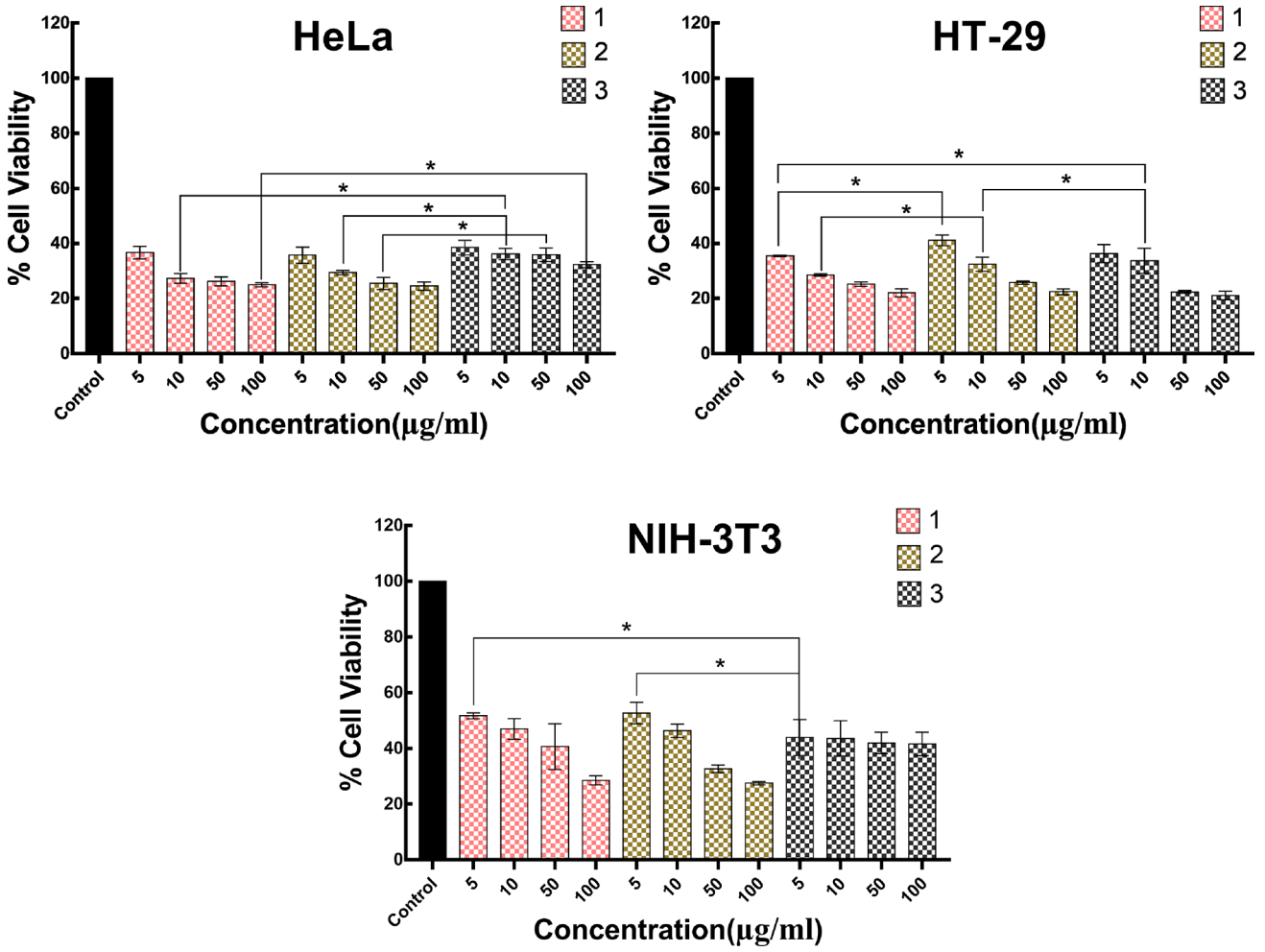

Figure 8. Cytotoxicity profile of **1**−**3** against HeLa, HT-29, and NIH-3T3 cells for 48 h, as determined by the MTT assay. Data are reported as the mean ± SD for n = 4 and (*) p < 0.05 statistical differences between treatment of complexes **1**, **2**, and **3**.

https://dx.doi.org/10.1021/acs.inorgchem.0c02563
Inorg. Chem. XXXX, XXX, XXX−XXX

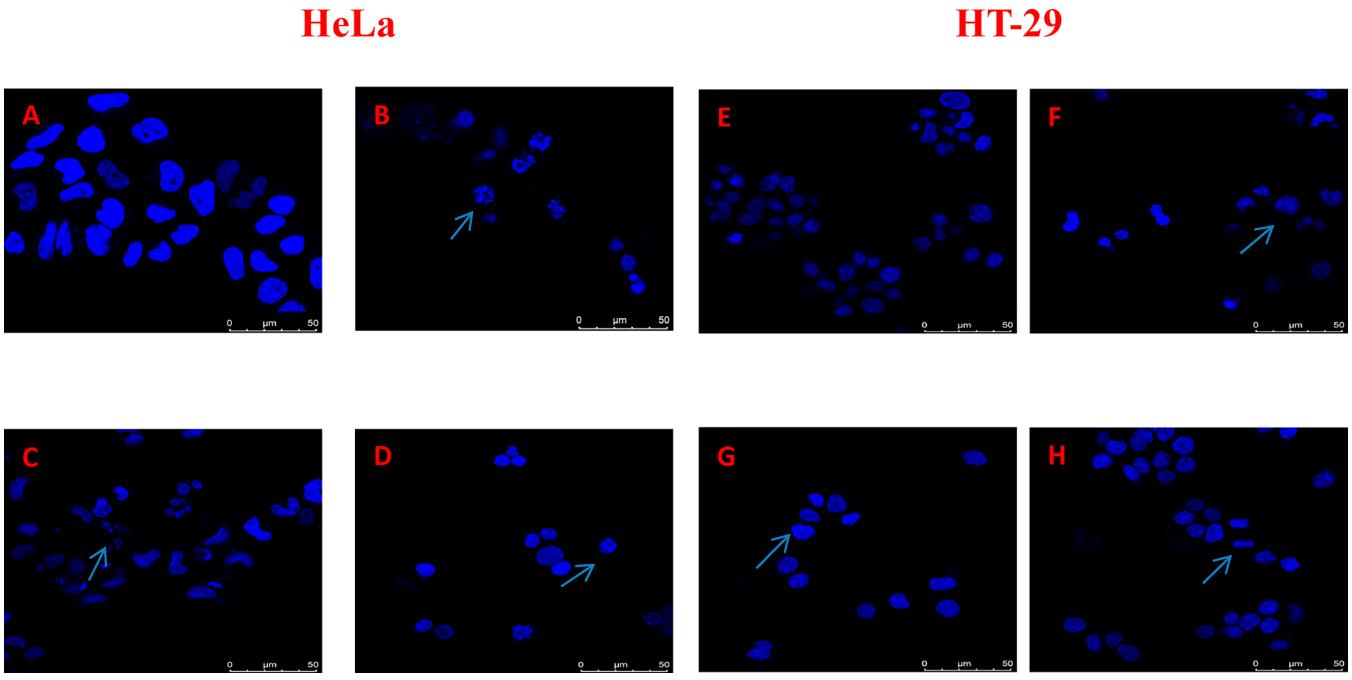

Figure 9. Morphology of HeLa (A) control, (B) **1**, (C) **2**, (D) **3** and HT-29 (E) control, (F) **1**, (G) **2**, (H) **3** cells treated with test complexes **1**−**3** at their IC_{50} values for 12 h. The cells were visualized under confocal microscope after Hoechst staining. The scale bar corresponds to 50 μm.

ruthenium(II) complexes (IC_{50} > 100−11.3 μM), reported by Liu and co-workers.[47] Moreover, complexes **1**−**3** show an improved cytotoxic activity against HT-29 cells as compared to vanadium arylazo systems (IC_{50} 28.8−25.9 μM), which were studied previously.[26a] These biological observations stress the importance of varying the metal center as well as the further tuning of the ligand environment in order to achieve higher antiproliferative activity.

Analysis of Nuclear Morphology with Hoechst Staining. Cell death can be initiated by two pathways, specifically, apoptosis and necrosis. In contrast to necrosis, apoptosis proceeds through a regulated pathway and is a programmed cell death[52] that includes chromatin condensation and nuclear fragmentation.[53] These events take place in a cell in response to treatment with test complexes and can be studied through staining with DNA binding fluorescence dyes.

As shown in Figure 9, the control cells (A and E) showed intact morphology without any nuclear condensation. However, cells treated with complexes **1**−**3** at concentrations around their IC_{50} values (B−D and F−H) revealed abnormal and fragmented nuclear morphology along with nuclear blebbings and condensed chromatin. Therefore, these complexes induce apoptosis in both HeLa and HT-29 cancer cells.

CONCLUSIONS

The chemistry of three new organometallic arylazo ruthenium(II) (**1** and **2**) and iridium(III) (**3**) complexes has been reported. Complexes **1**−**3** were fully characterized, including structural analysis by single-crystal X-ray diffraction. All of the complexes have a distorted octahedral geometry, whereby the two PPh_3 groups occupy the axial positions, and the sixth coordination site in the equatorial plane is occupied by the CO, CH_3CN, and H^- ligand in **1**, **2**, and **3**, respectively. Metal (Ru and Ir)-mediated C−H activation of the ligand occurs in all three complexes, resulting in coordination of the ligand as a tridentate, dianionic C, N, O-donor. In order to rationalize the CO formation and its coordination to the Ru(II) center in the case of **1**, a mechanism via alcohol dehydrogenation has been proposed. Furthermore, consistent with this proposed mechanism, a ^{13}CO-labeled complex (**1A**) could be synthesized using isotopically labeled ethanol, $CH_3{}^{13}CH_2OH$. Also, key intermediates could be identified through trapping in a coordinating solvent (CH_3CN) and comparison to an isoelectronic Ir complex. The cytotoxicity of our new complexes (IC_{50} values ∼4 μM) is significantly better than cisplatin under identical conditions. All three complexes induce cell death by apoptosis, as indicated by nuclear damage (fluorescence microscopy after staining with Hoechst dye). The results encourage further insights into the mechanistic aspects of cytotoxicity of this family of complexes, and tests on other cancer cell lines are the scope of future research. The ruthenium carbonyl complex $[RuL(PPh_3)_2CO]$ can act as a CO reservoir and therefore may be utilized for hydroformylation reactions or as a catalyst precursor for the reduction of CO_2 or the water gas shift reaction. There is thus scope for further research in this regard.

ASSOCIATED CONTENT

Supporting Information

The Supporting Information is available free of charge at https://pubs.acs.org/doi/10.1021/acs.inorgchem.0c02563.

Time-dependent absorption spectra, IR spectra, ESI-MS spectra, UV−vis spectra, ^1H NMR spectra, cyclic votammograms. CCDC numbers 1995381, 1995379, 1995380 correspond to **1**, **2**, and **3**, respectively (PDF)

Accession Codes

CCDC 1995379−1995381 contain the supplementary crystallographic data for this paper. These data can be obtained free of charge via www.ccdc.cam.ac.uk/data_request/cif, or by emailing data_request@ccdc.cam.ac.uk, or by contacting The

https://dx.doi.org/10.1021/acs.inorgchem.0c02563
Inorg. Chem. XXXX, XXX, XXX−XXX

Cambridge Crystallographic Data Centre, 12 Union Road, Cambridge CB2 1EZ, UK; fax: +44 1223 336033.

AUTHOR INFORMATION

Corresponding Authors

Nils Metzler-Nolte − *Department of Chemistry and Biochemistry, Ruhr University Bochum, Bochum 44801, Germany;* orcid.org/0000-0001-8111-9959; Email: nils.metzler-nolte@rub.de

Rupam Dinda − *Department of Chemistry, National Institute of Technology, Rourkela 769008, Odisha, India;* orcid.org/0000-0001-9452-7791; Email: rupamdinda@nitrkl.ac.in

Authors

Satabdi Roy − *Department of Chemistry, National Institute of Technology, Rourkela 769008, Odisha, India*

Monalisa Mohanty − *Department of Chemistry, National Institute of Technology, Rourkela 769008, Odisha, India*

Reece G. Miller − *Department of Chemistry and Biochemistry, Ruhr University Bochum, Bochum 44801, Germany;* orcid.org/0000-0002-2687-5572

Sushree Aradhana Patra − *Department of Chemistry, National Institute of Technology, Rourkela 769008, Odisha, India*

Sudhir Lima − *Department of Chemistry, National Institute of Technology, Rourkela 769008, Odisha, India*

Atanu Banerjee − *Department of Chemistry, National Institute of Technology, Rourkela 769008, Odisha, India*

Ekkehard Sinn − *Department of Chemistry, Western Michigan University, Kalamazoo 49008, Michigan, United States*

Werner Kaminsky − *Department of Chemistry, University of Washington, Seattle 98195, Washington, United States;* orcid.org/0000-0002-9100-4909

Complete contact information is available at: https://pubs.acs.org/10.1021/acs.inorgchem.0c02563

Author Contributions

The manuscript was written through contributions of all authors. All authors have given approval to the final version of the manuscript.

Notes

The authors declare no competing financial interest.

ACKNOWLEDGMENTS

R.D. thanks CSIR, Government of India [Grant No. 01(2963)/18/EMR-II], for funding this research. R.D. also thanks Prof. S. K. Chattopadhyay for fruitful discussion. R.G.M. acknowledges support from the Alexander von Humboldt Foundation through a postdoctoral fellowship.

REFERENCES

(1) Hartwig, J. F. *Organotransition Metal Chemistry, from Bonding to Catalysis;* University Science Books: New York, 2010.

(2) Tsuji, J. In *Organopalladium Chemistry for Organic Synthesis;* Negishi, E.-I., Ed.; Wiley: NY, 2002; Vol. 2, pp 2648−2653.

(3) Garralda, M. A. Aldehyde C-H activation with late transition metal organometallic compounds. Formation and reactivity of acyl hydrido complexes. *Dalton Trans.* **2009**, 3635−3645.

(4) Modak, A.; Deb, A.; Patra, T.; Rana, S.; Maity, S.; Maiti, D. A general and efficient aldehyde decarbonylation reaction by using a palladium catalyst. *Chem. Commun.* **2012**, *48*, 4253−4255.

(5) Patra, T.; Manna, S.; Maiti, D. Metal Mediated Deformylation Reactions: Synthetic and Biological Avenues. *Angew. Chem., Int. Ed.* **2011**, *50*, 12140−12142.

(6) Sabo-Etienne, S.; Grellier, M. Ruthenium: Inorganic & Coordination Chemistry. In *Encyclopedia of Inorganic Chemistry* [Online]; John Wiley & Sons, Ltd, 2006.

(7) Domazetis, G.; Tarpey, B.; Dolphin, D.; James, B. R. Catalytic decarbonylation of aldehydes using ruthenium(II) porphyrin systems. *J. Chem. Soc., Chem. Commun.* **1980**, 939−940.

(8) Iwai, T.; Fujihara, T.; Tsuji, Y. The iridium-catalyzed decarbonylation of aldehydes under mild conditions. *Chem. Commun.* **2008**, 6215−6217.

(9) (a) Schirmer, A.; Rude, M. A.; Li, X. Z.; Popova, E.; del Cardayre, S. B. Microbial biosynthesis of alkanes. *Science* **2010**, *329*, 559−562. (b) Rana, S.; Haque, R.; Santosh, G.; Maiti, D. Decarbonylative Halogenation by a Vanadium Complex. *Inorg. Chem.* **2013**, *52*, 2927−2932. (c) Akanksha; Maiti, D. Microwave-assisted palladium mediated decarbonylation reaction: synthesis of eulatachromene. *Green Chem.* **2012**, *14*, 2314−2320. (d) Rana, S.; Pandey, B.; Dey, A.; Haque, R.; Rajaraman, G.; Maiti, D. A Doubly Biomimetic Synthetic Transformation: Catalytic Decarbonylation and Halogenation at Room Temperature by Vanadium Pentoxide. *ChemCatChem* **2016**, *8*, 3367−3374. (e) Kundu, P. K.; Dhiman, M.; Modak, A.; Chowdhury, A.; Polshettiwar, V.; Maiti, D. Palladium Nanoparticles Supported on Fibrous Silica (KCC-1-PEI/Pd): A suitable Nanocatalyst for Decarbonylation Reactions. *ChemPlusChem* **2016**, *81*, 1142−1146. (f) Modak, A.; Rana, S.; Phukan, A. K.; Maiti, D. Palladium-Catalyzed Deformylation Reactions with Detailed Experimental and in Silico Mechanistic Studies. *Eur. J. Org. Chem.* **2017**, *2017*, 4168−4174. (g) Modak, A.; Naveen, T.; Maiti, D. An efficient dehydroxymethylation reaction by a palladium catalyst. *Chem. Commun.* **2013**, *49*, 252−254.

(10) Acharyya, R.; Peng, S.-M.; Lee, G. H.; Bhattacharya, S. An Unprecedented Oxidative Migration of a Methyl Group from 2-(2 ‘, 6 ‘-Dimethylphenylazo)-4-methylphenol Mediated by Ruthenium and Osmium. *Inorg. Chem.* **2003**, *42*, 7378−7380.

(11) Jayanthi, E.; Kalaiselvi, S.; Padma, V. V.; Bhuvanesh, N. S. P.; Dharmaraj, N. Solvent assisted formation of ruthenium(iii) and ruthenium(ii) hydrazone complexes in one-pot with potential *in vitro* cytotoxicity and enhanced LDH, NO and ROS release. *Dalton Trans.* **2016**, *45*, 1693−1707 and references therein.

(12) Dinger, M. B.; Mol, J. C. Degradation of the First-Generation Grubbs Metathesis Catalyst with Primary Alcohols, Water, and Oxygen. Formation and Catalytic Activity of Ruthenium(II) Monocarbonyl Species. *Organometallics* **2003**, *22*, 1089−1095.

(13) (a) Acharyya, R.; Basuli, F.; Wang, R.-Z.; Mak, T. C. W.; Bhattacharya, S. Iridium(III) complexes formed by O-H and/Or C-H activation of 2-(arylazo)phenols. *Inorg. Chem.* **2004**, *43*, 704−711. (b) Maiti, N.; Pal, S.; Chattopadhyay, S. Reaction of 2-(Phenylazo)-aniline with Na_2PdCl_4: Formation of a 2-(Phenylazo)imino Complex of Bivalent Palladium. *Inorg. Chem.* **2001**, *40*, 2204−2205. (c) Datta, P.; Sardar, D.; Saha, R.; Mondal, T. K.; Sinha, C. Structure, photophysics, electrochemistry and DFT calculations of [RuH(CO)-$(PPh_3)_2$(coumarinyl-azo-imidazole)]. *Polyhedron* **2013**, *53*, 193−201.

(14) (a) Krause, R. A.; Krause, K. Chemistry of bipyridyl-like ligands. Isomeric complexes of ruthenium(II) with 2-(phenylazo)-pyridine. *Inorg. Chem.* **1980**, *19*, 2600−2603. (b) Pratihar, J. L.; Bhaduri, S.; Pattanayak, P.; Patra, D.; Chattopadhyay, S. Reactions of 2-(arylazo)aniline with ruthenium substrates: Isolation, characterizations and reactivities of delocalized diazoketiminato and orthometallated Ru(II) chelates. *J. Organomet. Chem.* **2009**, *694*, 3401−3408. (c) Basu, S.; Halder, S.; Pal, I.; Samanta, S.; Karmakar, P.; Drew, M. G. B.; Bhattacharya, S. 1-(20-Pyridylazo)-2-naphtholate complexes of ruthenium: Synthesis, characterization, and DNA binding properties. *Polyhedron* **2008**, *27*, 2943−2951.

(15) (a) Ghosh, P.; Pramanik, A.; Bag, N.; Chakravorty, A. Bis(N, N) chelated rhenium(III): the $[ReL_2Cl_2]Cl$ family [L = 2-(arylazo)-pyridine]. *J. Chem. Soc., Dalton Trans.* **1992**, 1883−1886. (b) Lahiri, G. K.; Bhattacharya, S.; Goswami, S.; Chakravorty, A. High-potential isomeric ruthenium(III) complexes of 2-(phenylazo)pyridine. *J. Chem. Soc., Dalton Trans.* **1990**, 561−565. (c) Ghosh, B. K.; Chakravorty, A. Electrochemical studies of ruthenium compounds.

Part I. Ligand oxidation levels. *Coord. Chem. Rev.* **1989**, *95*, 239−294. (d) Wolfgang, S.; Strekas, T. C.; Gafney, H. D.; Krause, A. R.; Krause, K. Spectral and photophysical properties of ruthenium(II) 2-(phenylazo)pyridine complexes. *Inorg. Chem.* **1984**, *23*, 2650−2655. (e) Goswami, S.; Mukherjee, R. N.; Chakravorty, A. Chemistry of ruthenium. 12. Reactions of bidentate ligands with diaquabis[2-(arylazo)pyridine]ruthenium(II) cation. Stereoretentive synthesis of tris chelates and their characterization: metal oxidation, ligand reduction, and spectroelectrochemical correlation. *Inorg. Chem.* **1983**, *22*, 2825−2832. (f) Goswami, S.; Chakravarty, A. R.; Chakravorty, A. Chemistry of ruthenium. 7. Aqua complexes of isomeric bis[(2-arylazo)pyridine]ruthenium(II) moieties and their reactions: solvolysis, protic equilibriums, and electrochemistry. *Inorg. Chem.* **1983**, *22*, 602−609.

(16) (a) Ghosh, A. K.; Majumdar, P.; Falvello, L. R.; Mostafa, G.; Goswami, S. Novel Examples of Simultaneous Reductive Azo Cleavage and Oxidative Aromatic Ring Amination in Rhodium Complexes of 2-(Arylazo)pyridine. *Organometallics* **1999**, *18*, 5086−5090. (b) Lahiri, G. K.; Goswami, S.; Falvello, L. R.; Chakravorty, A. A new family of semibent rhenium(V) arylimides formed by azo splitting. Structure, bonding, and electrooxidation to rhenium(VI) congeners. *Inorg. Chem.* **1987**, *26*, 3365−3370. (c) Goswami, S.; Chakravarty, A. R.; Chakravorty, A. The aquaruthenium(II)-oxoruthenium(IV) couple in a ruthenium complex of 2-(phenylazo)-pyridine: homogeneous catalysis of the oxidation of water to dioxygen. *J. Chem. Soc., Chem. Commun.* **1982**, 1288−1289. (d) Goswami, S.; Chakravarty, A. R.; Chakravorty, A. Chemistry of ruthenium. 5. Reaction of trans-dihalobis[2-(arylazo)pyridine]-ruthenium(II) with tertiary phosphines: chemical, spectroelectrochemical, and mechanistic characterization of geometrically isomerized substitution products. *Inorg. Chem.* **1982**, *21*, 2737−2742.

(17) (a) Dougan, S. J.; Habtemariam, A.; McHale, S. E.; Parsons, S.; Sadler, P. J. Catalytic organometallic anticancer complexes. *Proc. Natl. Acad. Sci. U. S. A.* **2008**, *105*, 11628−11633. (b) Pazinato, J.; Cruz, O. M.; Naidek, K. P.; Pires, A. R. A.; Westphal, E.; Gallardo, H.; Baubichon-Cortay, H.; Rocha, M. E. M.; Martinez, G. R.; Winnischofer, S. M. B.; Di Pietro, A.; Winnischofer, H. Cytotoxicity of η^6-areneruthenium-based molecules to glioblastoma cells and their recognition by multidrug ABC transporters. *Eur. J. Med. Chem.* **2018**, *148*, 165−177. (c) Dougan, S. J.; Melchart, M.; Habtemariam, A.; Parsons, S.; Sadler, P. J. Phenylazopyridine and Phenylazo-pyrazole Chlorido Ruthenium(II) Arene Complexes: Arene Loss, Aquation, and Cancer Cell Cytotoxicity. *Inorg. Chem.* **2006**, *45*, 10882−10894. (d) Wang, D.; Lippard, S. J. Cellular Processing of platinum anticancer drugs. *Nat. Rev. Drug Discovery* **2005**, *4*, 307−320. (e) Dabrowiak, J. C. *Metals in Medicine;* John Wiley & Sons: Hoboken, NJ, 2013; pp 151−161. (f) Yao, X.; Panichpisal, K.; Kurtzman, N.; Nugent, K. Cisplatin Nephrotoxicity: A Review. *Am. J. Med. Sci.* **2007**, *334*, 115−124.

(18) (a) Kostova, I. Ruthenium complexes as anticancer agents. *Curr. Med. Chem.* **2006**, *13*, 1085−1107. (b) Gothe, Y.; Marzo, T.; Messori, L.; Metzler-Nolte, N. Cytotoxic activity and protein binding through an unusual oxidative mechanism by an iridium(I)-NHC complex. *Chem. Commun.* **2015**, *51*, 3151−3153. (c) Gothe, Y.; Marzo, T.; Messori, L.; Metzler-Nolte, N. Iridium(I) Compounds as Prospective Anticancer Agents: Solution Chemistry, Antiproliferative Profiles and Protein Interactions for a Series of Iridium(I) N-Heterocyclic Carbene Complexes. *Chem. - Eur. J.* **2016**, *22*, 12487−12494. (d) Gothe, Y.; Romero-Canelón, I.; Marzo, T.; Sadler, P. J.; Messori, L.; Metzler-Nolte, N. Synthesis and Mode of Action Studies on Iridium(I)-NHC Anticancer Drug Candidates. *Eur. J. Inorg. Chem.* **2018**, *2018*, 2461−2470.

(19) Hartinger, C. G.; Jakupec, M. A.; Zorbas-Seifried, S.; Groessl, M.; Egger, A.; Berger, W.; Zorbas, H.; Dyson, P. J.; Keppler, B. K. KP1019, a new redox-active anticancer agent–preclinical development and results of a clinical phase I study in tumor patients. *Chem. Biodiversity* **2008**, *5*, 2140−2155.

(20) Dickson, N. R.; Jones, S. F.; Burris, H. A.; Ramanathan, R. K.; Weiss, G. J.; Infante, J. R.; Bendell, J. C.; McCulloch, W.; Von Hoff, D. D. A Phase I Dose Escalation Study of NKP-1339 in Patients with Advanced Solid Tumors Refractory to Treatment. *J. Clin. Oncol.* **2011**, *29*, 2607 (suppl., abstr.).

(21) Enzo Alessio; Giovanni Mestroni; Alberta Bergamo; Gianni Sava. Ruthenium antimetastatic agents. *Curr. Top. Med. Chem.* **2004**, *4*, 1525−1535.

(22) Henze, K.; Martin, W. Evolutionary biology: essence of mitochondria. *Nature* **2003**, *426*, 127−128.

(23) McBride, H. M.; Neuspiel, M.; Wasiak, S. Mitochondria: more than just a powerhouse. *Curr. Biol.* **2006**, *16*, 551−560.

(24) Youle, R. J.; Narendra, D. P. Mechanisms of mitophagy. *Nat. Rev. Mol. Cell Biol.* **2011**, *12*, 9−14.

(25) (a) Ganguly, D.; Jain, C. K.; Santra, R. C.; Roychoudhury, S.; Majumder, H. K.; Das, S. The biological *in vitro* effect and selectivity shown by a Co^{II} complex of 2-(2-hydroxyphenylazo)-indole-3′-acetic acid on three distinctly different cancer cells. *RSC Adv.* **2017**, *7*, 3428−3428. (b) Venugopal, N.; Krishnamurthy, G.; Bhojyanaik, H. S.; Giridhar, M. Novel bioactive azo-azomethine based Cu (II), Co (II) and Ni(II) complexes, structural determination and biological activity. *J. Mol. Struct.* **2019**, *1191*, 85−94.

(26) (a) Roy, S.; Böhme, M.; Dash, S. P.; Mohanty, M.; Buchholz, A.; Plass, W.; Majumder, S.; Kulanthaivel, S.; Banerjee, I.; Reuter, H.; Kaminsky, W.; Dinda, R. Anionic Dinuclear Oxidovanadium(IV) Complexes with Azo Functionalized Tridentate Ligands and μ-Ethoxido Bridge Leading to an Unsymmetric Twisted Arrangement: Synthesis, X-ray Structure, Magnetic Properties, and Cytotoxicity. *Inorg. Chem.* **2018**, *57*, 5767−5781. (b) Lima, S.; Banerjee, A.; Mohanty, M.; Sahu, G.; Kausar, C.; Patra, S. K.; Garribba, E.; Kaminsky, W.; Dinda, R. Synthesis, structure and biological evaluation of mixed ligand oxidovanadium(IV) complexes incorporating 2-(arylazo)phenolates. *New J. Chem.* **2019**, *43*, 17711−17725.

(27) (a) Li, S.; Zhao, J.; Guo, Y.; Mei, Y.; Yuan, B.; Gan, N.; Zhang, J.; Hu, J.; Hou, H. Influence of the introduction of a mitochondrion-targeting group on the anticancer activity of a copper complex. *J. Inorg. Biochem.* **2020**, *210*, 111102−111111. (b) Chen, Z. G.; Kang, X. X.; Wu, Y. X.; Xiao, H. H.; Cai, X. Z.; Sheng, S. H.; Wang, X. F.; Chen, S. G. A Mitochondria Targeting Artesunate Prodrug Loaded Nanoparticle Exerting Anticancer Activity via Iron-Mediated Generation of Reactive Oxygen Species. *Chem. Commun.* **2019**, *55*, 4781−4784. (c) Wang, K.; Zhu, C. C.; He, Y. F.; Zhang, Z. Q.; Zhou, W.; Muhammad, N.; Guo, Y.; Wang, X. Y.; Guo, Z. J. Restraining Cancer Cells by Dual-Metabolic Inhibitions with a Mitochondrion-Targeted Platinum(II) Complex. *Angew. Chem., Int. Ed.* **2019**, *58*, 4638−4643. (d) Chrysouli, M.P.; Banti, C.N.; Kourkoumelis, N.; Panayiotou, N.; Markopoulos, G.S.; Tasiopoulos, A.J.; Hadjikakou, S.K. Chloro-(triphenylphosphine)gold(I) a forefront reagent in gold chemistry as apoptotic agent for cancer cell. *J. Inorg. Biochem.* **2018**, *179*, 107−120. (e) De Nisi, A.; Bergamini, C.; Leonzio, M.; Sartor, G.; Fato, R.; Naldi, M.; Monari, M.; Calonghi, N.; Bandini, M. Synthesis, cytotoxicity and anticancer activity of new alkynyl-gold(I) complexes. *Dalton Trans.* **2016**, *45*, 1546−1553. (f) Castonguay, A.; Doucet, C.; Juhas, M.; Maysinger, D. New Ruthenium(II)-Letrozole Complexes as Anticancer Therapeutics. *J. Med. Chem.* **2012**, *55*, 8799−8806. (g) Jin, S. X.; Hao, Y. G.; Zhu, Z. Z.; Muhammad, N.; Zhang, Z. Q.; Wang, K.; Guo, Y.; Guo, Z. J.; Wang, X. Y. Impact of Mitochondrion-Targeting Group on the Reactivity and Cytostatic Pathway of Platinum(IV) Complexes. *Inorg. Chem.* **2018**, *57*, 11135−11145. (h) Ribeiro, G. H.; Colina-Vegas, L.; Clavijo, J. C.T.; Ellena, J.; Cominetti, M. R.; Batista, A. A. Ru(II)/N-N/PPh3 complexes as potential anticancer agents against MDAMB- 231 cancer cells (N-N = diimine or diamine). *J. Inorg. Biochem.* **2019**, *193*, 70−83 and references therein. (i) Villarreal, W.; Colina-Vegas, L.; Rodrigues de Oliveira, C.; Tenorio, J. C.; Ellena, J.; Gozzo, F. C.; Cominetti, M. R.; Ferreira, A. G.; Ferreira, M. A. B.; Navarro, M.; Batista, A. A. Chiral Platinum(II) Complexes Featuring Phosphine and Chloroquine Ligands as Cytotoxic and Monofunctional DNA-Binding Agents. *Inorg. Chem.* **2015**, *54*, 11709−11720. (j) Saez, R.; Lorenzo, J.; Prieto, M. J.; Font-Bardia, M.; Calvet, T.; Omenaca, N.; Vilaseca, M.; Moreno, V. Influence of PPh_3 moiety in the anticancer activity of new

https://dx.doi.org/10.1021/acs.inorgchem.0c02563
Inorg. Chem. XXXX, XXX, XXX−XXX

organometallic ruthenium complexes. *J. Inorg. Biochem.* **2014**, *136*, 1−12. (k) Bomfim, L. M.; de Araujo, F. A.; Dias, R. B.; Sales, C. B. S.; Rocha, C. A. G.; Correa, R. S.; Soares, M. B. P.; Batista, A. A.; Bezerra, D. P. Ruthenium(II) complexes with 6-methyl-2-thiouracil selectively reduce cell proliferation, cause DNA double-strand break and trigger caspase-mediated apoptosis through JNK/p38 pathways in human acute promyelocytic leukemia cells. *Sci. Rep.* **2019**, *9*, 11483. (l) Papazoglou, I.; Cox, P. J.; Hatzidimitriou, A. G.; Kokotidou, C.; Choli-Papadopoulou, T.; Aslanidis, P. Copper(I) halide complexes of 5-carbethoxy-2-thiouracil: Synthesis, structure and in vitro cytotoxicity. *Eur. J. Med. Chem.* **2014**, *78*, 383−391. (m) Hadjikakou, S. K.; Aslanidis, P.; Karagiannidis, P.; Kojic-Prodic, B.; Luic, M. Preparation and spectral studies of dinuclear mixed-ligand copper(I) complexes. The crystal structure of bis[m-s(pyridine-2-thione)(tmtp) copper(I) bromide]. *Polyhedron* **1994**, *13*, 3119−3125. (n) González-Alvarez, M.; Alzuet, G.; Borrás, J.; García-Granda, S.; Montejo- Bernardo, J. M. Structural and functional models for the dinuclear copper active site in catechol oxidases. Synthesis, X-ray crystal structures, magnetic and spectroscopic properties of m-methoxo-bridged dinuclear copper(II) complexes with N-substituted sulfonamide ligands. *J. Inorg. Biochem.* **2003**, *96*, 443−451. (o) Stromyer, M. L.; Southerland, M. R.; Satyal, U.; Sikder, R. K.; Weader, D. J.; Baughman, J. A.; Youngs, W. J.; Abbosh, P. H. Synthesis, characterization, and biological activity of a triphenylphosphonium-containing imidazolium salt against select bladder cancer cell lines. *Eur. J. Med. Chem.* **2020**, *185*, 111832−111841. (p) Biancalana, L.; Zacchini, S.; Ferri, N.; Lupo, M. G.; Pampaloni, G.; Marchetti, F. Tuning the cytotoxicity of ruthenium(II) paracymene complexes by mono-substitution at a triphenylphosphine/phenoxydiphenylphosphine ligand. *Dalton Trans.* **2017**, *46*, 16589−16604. (q) Barreiro, E.; Casas, J. S.; Couce, M. D.; Sánchez, A.; Sánchez-González, A.; Sordo, J.; Varela, J. M.; Vazquez López, E. M. Dinuclear triphenylphosphinegold(I) sulfanylcarboxylates: Synthesis, structure and cytotoxic activity against cancer cell lines. *J. Inorg. Biochem.* **2010**, *104*, 551−559.

(28) Hallman, P. S.; Stephenson, T. A.; Wilkinson, G. Tetrakis-(triphenylphosphine)dichlororuthenium(II) and Tris-(triphenylphosphine)dichlororuthenium(II). In *Inorganic Syntheses;* John Wiley & Sons, Inc., 2007; pp 237−240.

(29) Baksi, S.; Acharyya, R.; Dutta, S.; Blake, A. J.; Drew, M. G. B.; Bhattacharya, S. Interaction of 2-(arylazo) phenols with rhodium. Usual coordination vs. C-H and C-C activation. *J. Organomet. Chem.* **2007**, *692*, 1025−1032 and references therein.

(30) *SAINT;* Bruker AXS Inc.: Madison, WI, 2008.

(31) *SADABS;* Bruker AXS Inc.: Madison, WI, 2008.

(32) Sheldrick, G. M. Crystal structure refinement with SHELXL. *Acta Cryst.* 2015 C71, 3−8.

(33) Wang, X.; Tanaka, M.; Krstin, S.; Peixoto, H. S.; Moura, C. C. d. M.; Wink, M. Cytoskeletal interference - A new mode of action for the anticancer drugs camptothecin and topotecan. *Eur. J. Pharmacol.* **2016**, *789*, 265−274.

(34) (a) Gupta, P.; Dutta, S.; Basuli, F.; Peng, S.-M.; Lee, G.-H.; Bhattacharya, S. Ruthenium Mediated C- H Activation of 2-(Arylazo) phenols: Characterization of an Intermediate and the Final Organoruthenium Complex. *Inorg. Chem.* **2006**, *45*, 460−467. (b) Mandal, S.; Samanta, S.; Mondal, T. K.; Goswami, S. Activation in *ortho*-$C_{aromatic}$-N Bond Fusion in Substituted Anilines Using Ruthenium(II) Mediators: Isolation and Characterization of Unusual Ru_2 Complexes. *Organometallics* **2012**, *31*, 5282−5293. (c) Acharyya, R.; Basuli, F.; Peng, S.-M.; Lee, G.-H.; Wang, R.-Z.; Mak, T. C. W.; Bhattacharya, S. Iridium mediated methyl and phenyl C-H activation of 2-(arylazo)-phenols. Synthesis, structure, and spectral and electrochemical properties of some organoiridium complexes. *J. Organomet. Chem.* **2005**, *690*, 3908−3917.

(35) Nag, S.; Gupta, P.; Butcher, R. J.; Bhattacharya, S. Unprecedented Migration of a Methyl Group in 2-(2 ', 6 '-Dimethylphenylazo)-4-methylphenol Mediated by Ruthenium. *Inorg. Chem.* **2004**, *43*, 4814−4816.

(36) Acharyya, R.; Peng, S.-M.; Lee, G.-H.; Bhattacharya, S. Iridium mediated phenolic OH activation and cyclometalation of 2-(naphthyl-1'-azo)-4-methylphenol—Formation of organoiridium complexes. *J. Chem. Sci.* **2009**, *121*, 387−395.

(37) Yi, C. S.; Lee, D. W.; Chen, Y. Hydrovinylation and [2+ 2] Cycloaddition Reactions of Alkynes and Alkenes Catalyzed by a Well-Defined Cationic Ruthenium-Alkylidene Complex. *Organometallics* **1999**, *18*, 2043−2045.

(38) (a) Ghosh, P.; Bag, N.; Chakravorty, A. Decarbonylative Metalation of Diformylphenol Schiff Bases: New Osmium and Ruthenium Organometallics Incorporating the Iminium- Phenolato Zwitterionic Motif. *Organometallics* **1996**, *15*, 3042−3047. (b) Bag, N.; Choudhury, S. B.; Pramanik, A.; Lahiri, G. K.; Chakravorty, A. Ruthenium (II) phenolates. Synthesis and characterization of a novel four-membered metallacycle. *Inorg. Chem.* **1990**, *29*, 5013−5014.

(39) Fristrup, P.; Kreis, M.; Palmelund, A.; Norrby, P.-O.; Madsen, R. The mechanism for the rhodium-catalyzed decarbonylation of aldehydes: a combined experimental and theoretical study. *J. Am. Chem. Soc.* **2008**, *130*, 5206−5215.

(40) Modak, A.; Maiti, D. Metal catalyzed defunctionalization reactions. *Org. Biomol. Chem.* **2016**, *14*, 21−35.

(41) Halder, S.; Drew, M. G. B.; Bhattacharya, S. Palladium and platinum complexes of 2-(2'-carboxyphenylazo)-4-methylphenol: Synthesis, structure and spectral properties. *J. Chem. Sci.* **2008**, *120*, 441−446.

(42) Panda, M.; Paul, N. D.; Joy, S.; Hung, C.-H.; Goswami, S. Hydrido iridium (III) complexes of azoaromatic ligands. Isolation, structure and studies of their physicochemical properties. *Inorg. Chim. Acta* **2011**, *372*, 168−174.

(43) Lo, K. K. -W.; Chung, C.-K.; Zhu, N. Synthesis, Photophysical and Electrochemical Properties, and Biological Labeling Studies of Cyclometalated Iridium(III) Bis(pyridylbenzaldehyde) Complexes: Novel Luminescent Cross Linkers for Biomolecules. *Chem. - Eur. J.* **2003**, *9*, 475−483.

(44) Djukic, M.; Jeremic, M. S.; Jelic, R.; Klisuric, O.; Kojic, V.; Jakimov, D.; Djurdjevic, P.; Matovic, Z. D. Further insights into ruthenium(II) piano-stool complexes with *N*-alkylimidazoles. *Inorg. Chim. Acta* **2018**, *483*, 359−370.

(45) Chang, S. W.; Lewis, A. R.; Prosser, K. E.; Thompson, J. R.; Gladkikh, M.; Bally, M. B.; Warren, J. J.; Walsby, C. J. CF_3 Derivatives of the Anticancer Ru(III) Complexes KP1019, NKP-1339, and Their Imidazole and Pyridine Analogues Show Enhanced Lipophilicity, Albumin Interactions, and Cytotoxicity. *Inorg. Chem.* **2016**, *55*, 4850−4863.

(46) Yang, Y.; Ge, X.; Guo, L.; Zhu, T.; Tian, Z.; Zhang, H.; Du, Q.; Peng, H.; Ma, W.; Liu, Z. Zwitterionic and cationic half-sandwich iridium(iii) ruthenium(ii) complexes bearing sulfonate groups: synthesis, characterization and their different biological activity. *Dalton Trans.* **2019**, *48*, 3193−3197.

(47) Ma, W.; Zhang, S.; Tian, Z.; Xu, Z.; Zhang, Y.; Xia, X.; Chen, X.; Liu, Z. Potential anticancer agent for selective damage to mitochondria or lysosomes: Naphthalimide-modified fluorescent biomarker half-sandwich iridium (III) and ruthenium (II) complexes. *Eur. J. Med. Chem.* **2019**, *181*, 111599−111608.

(48) Avaji, P. G.; Vinod Kumar, C. H.; Patil, S. A.; Shivananda, K. N.; Nagaraju, C. Synthesis, spectral characterization, in-vitro microbiological spectral evaluation and cytotoxic activities of novel macrocyclic bis hydrazone. *Eur. J. Med. Chem.* **2009**, *44*, 3552−3559.

(49) (a) Saswati, S.; Adão, P.; Majumder, S.; Dash, S. P.; Roy, S.; Kuznetsov, M.; Costa Pessoa, J.; Gomes, C. S. B.; Hardikar, M. R.; Tiekink, E. R.T.; Dinda, R. Synthesis, structure, solution behavior, reactivity and biological evaluation of oxidovanadium(IV/V) thiosemicarbazone complexes. *Dalton Trans.* **2018**, *47*, 11358−11374. (b) Majumder, S.; Pasayat, S.; Panda, A. K.; Dash, S. P.; Roy, S.; Biswas, A.; Varma, M. E.; Joshi, B. N.; Garribba, E.; Kausar, C.; Patra, S. K.; Kaminsky, W.; Crochet, A.; Dinda, R. Monomeric and Dimeric Oxidomolybdenum(V and VI) Complexes, Cytotoxicity, and DNA Interaction Studies: Molybdenum Assisted C = N Bond Cleavage of Salophen Ligands. *Inorg. Chem.* **2017**, *56*, 11190−11210 and references therein. (c) Roy, S.; Mohanty, M.; Pasayat, S.; Majumder, S.; Senthilguru, K.; Banerjee, I.; Reichelt, M.; Reuter, H.;

https://dx.doi.org/10.1021/acs.inorgchem.0c02563
Inorg. Chem. XXXX, XXX, XXX−XXX

Sinn, E.; Dinda, R. Synthesis, structure and cytotoxicity of a series of Dioxidomolybdenum(VI) complexes featuring Salan ligands. *J. Inorg. Biochem.* **2017**, *172*, 110−121. (d) Dash, S. P.; Pasayat, S.; Bhakat, S.; Roy, S.; Dinda, R.; Tiekink, E. R. T.; Mukhopadhyay, S.; Bhutia, S. K.; Hardikar, M. R.; Joshi, B. N.; Patil, Y. P.; Nethaji, M. Highly Stable Hexacoordinated Nonoxidovanadium(IV) Complexes of Sterically Constrained Ligands: Syntheses, Structure, and Study of Antiproliferative and Insulin Mimetic Activity. *Inorg. Chem.* **2013**, *52*, 14096−14107.

(50) (a) Ruiz, J.; Rodriguez, V.; Cutillas, N.; Samper, K. G.; Capdevila, M.; Palacios, O.; Espinosa, A. Novel C, N-chelate rhodium(III) and iridium(III) antitumor complexes incorporating a lipophilic steroidal conjugate and their interaction with DNA. *Dalton Trans.* **2012**, *41*, 12847−12856. (b) El-Ghamry, H. A.; Fathalla, S. K.; Gaber, M. Synthesis, structural characterization and molecular modelling of bidentate azo dye metal complexes: DNA interaction to antimicrobial and anticancer activities. *Appl. Organomet. Chem.* **2018**, *32*, 4136−4148.

(51) (a) Reytman, L.; Braitbard, O.; Tshuva, E. Y. Highly cytotoxic vanadium(v) complexes of salan ligands; insights on the role of hydrolysis. *Dalton Trans.* **2012**, *41*, 5241−5247 and references therein. (b) Stockert, A.; Kinder, D.; Christ, M.; Amend, K.; Aulthouse, A. Improving the Efficacy of Cisplatin in Colon Cancer HT-29 Cells via Combination Therapy with Selenium. *Austin J. Pharmacol. Ther.* **2014**, *2*, 6−12. (c) Lewis, A. D.; Forrester, L. M.; Hayes, J. D.; Wareing, C. J.; Carmichael, J.; Harris, A. L.; Mooghen, M.; Wolf, C. R. Glutathione S-transferase isoenzymes in human tumors and tumor derived cell-lines. *Br. J. Cancer* **1989**, *60*, 327−331. (d) Takara, K.; Sakaeda, T.; Yagami, T.; Kobayashi, H.; Ohmoto, N.; Horinouchi, M.; Nishiguchi, K.; Okumura, K. Cytotoxic effects of 27 anticancer drugs in HeLa and MDR1-overexpressing derivative cell lines. *Biol. Pharm. Bull.* **2002**, *25*, 771−778. (e) Petinari, L.; Kohn, L. K.; de Carvalho, J. E.; Genari, S. C. Cytotoxicity of tamoxifen in normal and tumoral cell lines and its ability to induce cellular transformation in vitro. *Cell Biol. Int.* **2004**, *28*, 531−539.

(52) Ziegler, U.; Groscurth, P. Morphological features of cell death. *Physiology* **2004**, *19*, 124−128.

(53) Bezabeh, T.; Mowat, M. R. A.; Jarolim, L.; Greenberg, A. H.; Smith, I. C. P. Detection of drug-induced apoptosis and necrosis in human cervical carcinoma cells using ^{1}H NMR spectroscopy. *Cell Death Differ.* **2001**, *8*, 219−224.

https://dx.doi.org/10.1021/acs.inorgchem.0c02563
Inorg. Chem. XXXX, XXX, XXX−XXX